The Dissertation Committee for Sivaramakrishnan Swaminathan certifies that this is the approved version of the following dissertation:

Aspects of new physics beyond the Standard Model: electroweak naturalness, dark matter and holographic quantum gravity

Committee:

Can Kilic, Supervisor

Jacques Distler

Vadim Kaplunovsky

Sonia Paban

Paul Shapiro

Aspects of new physics beyond the Standard Model: electroweak naturalness, dark matter and holographic quantum gravity

by

Sivaramakrishnan Swaminathan

Dissertation

Presented to the Faculty of the Graduate School of

The University of Texas at Austin

in Partial Fulfillment

of the Requirements

for the degree of

Doctor of Philosophy

The University of Texas at Austin

August, 2017

Dedicated to my family.

Acknowledgments

On reflection, I realize how lucky I am to have had Can Kilic as my advisor. I sincerely thank him for taking on a rudderless student (me!) and guiding me through the process of research—from reading papers, to writing them, and everything in between. He has given direction to my research with his active participation, while always encouraging me to explore the breadth of my intellectual interests.

For making the process of research enjoyable and exciting, I would like to thank all my collaborators: Can Kilic (my advisor) and Prateek Agrawal, for sharing many insights about particle phenomenology and model building; Cynthia Trendafilova, for many late night internet chats while we cross-checked each other's calculations; Bartek Czech, for sharing his insights and showing me an opportunity to work on ideas at the interface of quantum gravity, renormalization group flow and quantum information; and Phuc Nguyen, for many Sundays spent working together at coffee shops, which eased me into research in the subject of holography.

I am grateful to the faculty members of the Theory Group for creating a free and collaborative research atmosphere. In particular, I would like to thank Jacques Distler, Sonia Paban, Vadim Kaplunovsky and Elena Caceres for numerous stimulating discussions and insights. I would also like to thank the Texas Cosmology Center journal club participants, in particular Paul Shapiro and Tom Crawford, for the opportunity to learn some cosmology through osmosis.

I would also like to thank Larry Shepley—for sharing his wisdom and unique brand of liveliness in Whizkey Seminar discussions, and Austin Gleeson—for encouraging me to design my own rendition of a Physical Science course and inspiring me to strive

towards communicating physics concepts in simple ways.

For many itinerant conversations on a wide variety of topics in physics (some under the banner of the 'Whizkey seminar') I would like to thank my fellow and senior colleagues, including: Akarsh Simha, Matthew Klimek, Victor Chua, Timothy Magee, Aaron Fenyes, Manasvi Lingam, Andy Trimm, Aswin Balasubramanian, Daniel Carney, Dustin Lorshbough, Aditya Aravind, Phuc Nguyen, Brandon DiNunno, Cynthia Trendafilova, Yuan-pao Yang, Ravi Mohan, George Miloshevich and Chris Reilly. By giving me opportunities to share my insights, my junior colleagues Niral Desai and Qianyu Hao helped me appreciate that many concepts I now understand once seemed utterly impenetrable to me, and that one can learn a lot without consciously realizing it, even when progress appears glacial. I consider myself fortunate for having had the opportunity to interact with such an enthusiastic peer group in graduate school.

I thank Jan Duffy and Matt Ervin for helping tame the bureaucratic complexities of the graduate school experience, so that students may focus on their work.

For making my extended visit to the Perimeter Institute a productive one, and for helping me along in my quest to understand tensor networks, I sincerely thank Guifre Vidal, Markus Hauru, Ashley Milsted and Qi Hu. I would like to also thank all my friends there for making it an enjoyable visit overall.

Spending a semester away made me realize that among all the aspects that make Austin great, it was my friends that I missed the most. For keeping my personal life fulfilling and exciting over the last several years, I would like to thank Akila Kesavasamy, Akarsh Simha, Kumar Appaiah, Karthikeyan Shanmugam, Salomi Naik, Prakash Mohan, Adithi Ramanan, and Subhash Chandra. I am grateful for their friendship and support, and to Akila, in particular, for helping create a cocoon of emotional abundance.

Reaching back into the years, among all the teachers I am grateful to, I would like to specifically mention Suresh Govindarajan—for mentoring me, teaching me a good chunk of the physics I know, and encouraging me to pursue doctoral studies. Given my academic beginnings as an undergraduate with youthful ideals, majoring in electrical engineering, pursuing advanced studies in physics would have been near impossible without his guidance.

The long journey in my adventure begins at home. For their constant love and support, encouraging my diverse interests, I am grateful to my parents. The role played by my grandparents and uncles in nurturing my curiosity cannot be overstated. My brother deserves a special mention for helping keep me grounded in spite of my theoretical pursuits. It is difficult to articulate their numerous influences and contributions that blended together in shaping the person I am—for which I dedicate this document to them.

This material is based upon work supported by the National Science Foundation under Grant Number PHY-1620610.

Aspects of new physics beyond the Standard Model: electroweak naturalness, dark matter and holographic quantum gravity

Publication No. _____

Sivaramakrishnan Swaminathan, Ph.D.
The University of Texas at Austin, 2017

Supervisors: Can Kilic

This dissertation is based on studies of three aspects of physics beyond the Standard Model. First, we summarize a study of high temperature symmetry restoration in extensions of the Standard Model where the naturalness problem is resolved due to the Higgs being a pseudo-Nambu-Goldstone boson. Second, we analyze a framework for building quantum field theoretic models where dark matter has its cosmic origins in an asymmetry, while the overall dark charge is conserved and the dark matter relic is actually symmetric at late times. Finally, we study the relation between holographic 'bulk' geometry, and the structure of entanglement in the quantum field theory living on the boundary as characterized by the Multiscale Entanglement Renormalization Ansatz (MERA).

Contents

List of Figures

Chapter One: The Standard Model and its discontents

The field of elementary particle physics has two antecedent threads traced back to the beginning of the twentieth century. One is the search for elementary particles describing all aspects of nature, starting with Rutherford's discovery of the internal structure of the atom. The other is the search for symmetry principles to constrain the physics of processes, as exploited in Einstein's formulation of electrodynamics as a theory with (what we now call) Lorentz invariance. These intertwining threads have led to the Standard Model of particle physics describing the electroweak and strong interactions by a quantum field theory with $SU(3) \times SU(2) \times U(1)$ gauge symmetry, and the General Theory of Relativity describing gravity through diffeomorphism invariance. As of the turn of the twentieth century, the existence of the Higgs boson was the only major piece of the Standard Model that was yet to be experimentally verified. With its recent discovery [10, 11], our description of electroweak symmetry breaking is now complete, and with it, the Standard Model.

Seen another way, the success of the Standard Model is a testament to the success of quantum field theory in describing in a unified manner, several aspects of fundamental physics. In the rest of this chapter, we shall consider three specific questions motivating further research at this frontier.

1.1 The quest for unification

The first example corresponds to unifying all known interactions in a manner similar to the unification of electricity and magnetism. While the Standard Model brought together the non-gravitational forces into the same framework, they still correspond to a priori unrelated gauge groups and couplings. One of the goals of unification would be to explain the gauge structure of the Standard Model, and the relation between the couplings, as measured at low energies. Some of the best studied models accomplishing this correspond to "Grand Unified Theories" (GUTs). In these models, the electroweak sector and the strong force stem from a single integrated gauge symmetry which was broken at a scale of around 10^{16}GeV, therefore called the "GUT" scale.

A more ambitious endeavor is to unify the description of gravity with our quantum mechanical model for the other forces. However, formulating a consistent and complete quantum mechanical theory of gravity is an open problem. Arguably, the best candidates to understand the structure of quantum gravity are holographic theories, where quantum gravity is expected to have a dual description in terms of quantum field theories in one lower spatial dimension. The most studied example [12–14] of this class is quantum gravity on AdS_5 which is dual to $\mathcal{N} = 4$ Supersymmetric Yang-Mills theory for a gauge group with a large number of generators and a large 't Hooft coupling. Several aspects of this correspondence (known commonly as 'AdS/CFT') are still to be understood fully, and recent developments have shown that the emergence of bulk space-time is intimately tied to the structure of entanglement among the degrees of freedom in the boundary quantum field theory. Tensor network constructions used to model many-body quantum states—such as the Multi-scale Entanglement Renormalization Ansatz (MERA)—are also motivated by principled reasoning about

the structure of entanglement. This motivates an exploration of the correspondence between tensor networks and the holographic geometry of space-time, to clarify the role of entanglement in the AdS/CFT correspondence. This forms the context for the work expounded in Chapter 4.

In that chapter, we study how tensor networks reproduce properties of static holographic space-times, which are not locally pure anti-de Sitter. We consider geometries that are holographically dual to ground states of CFTs with reduced symmetry (such as defect, interface and boundary CFTs) and compare them to the structure of the requisite MERA networks predicted by the theory of minimal updates. When the CFT is deformed, certain tensors in its MERA representation require updating. On the other hand, even identical tensors can contribute differently to estimates of entanglement entropies. We interpret these facts holographically by associating tensor updates to turning on non-normalizable modes in the bulk. We clarify and complement existing arguments in support of the theory of minimal updates. We also propose an ansatz called 'rayed MERA' that applies to a class of generalized interface CFTs, and analyze the kinematic spaces of the thin wall and AdS_3-Janus geometries.

1.2 Electroweak naturalness in the Standard Model

The second example, often referred to as the 'hierarchy problem' or the 'naturalness problem' or the 'finetuning problem', is the question of the (in)stability of one Standard Model parameter under renormalization group flow from scales in the deep ultraviolet, to the coarser scales probed in experiments. The low-energy effective value of most Standard Model parameters are not highly sensitive to their ultravio-

let values, since they do not receive large additive corrections under renormalization group flow. However, given the known symmetries of the Standard Model, the measured value of its only dimensionful parameter—corresponding to the background expectation value of the Higgs field[1] in the vacuum state, is surprising. To obtain the low-energy value matching experiments, it's value at ultraviolet scales must be precisely chosen to cancel large additive cutoff-dependent corrections during the flow, thereby exposing it to a 'finetuning problem'. In other words, the observed hierarchy between the electroweak vacuum and high energy scales forming plausible cutoffs for the Standard Model, such as the Planck scale (where quantum mechanical effects of gravity become important) or the "GUT"energy scale, is puzzling. It is worth emphasizing that this question is is not driven by an issue of consistency, but instead by a desire to have phenomenology not depend sensitively on the initial conditions of renormalization group flow.

Many mechanisms have been proposed to explain this fact, typically extending the electroweak sector with more degrees of freedom and symmetries. Among the most popular extensions is supersymmetry, which posits an opposite-statistics partner for each particle in the Standard Model, thereby pairing fermions with bosons. Other well-studied examples where Standard Model particles have same-spin (and same statistics) partners have the Higgs boson be a pseud-Nambu-Goldstone boson of some internal symmetry.

In such extensions of the Standard Model, where loop corrections to the Higgs potential cancel between Standard Model degrees of freedom and their symmetry partners, it is interesting to contemplate whether corresponding contributions to the finite temperature effective potential also cancel, which raises the question of whether

[1]The mass of the Higgs particle is expected to be relate to, and similar to the scale of its vacuum expectation value (VEV), as confirmed by its recent experimental measurement [10, 11].

a broken phase of electroweak symmetry may persist at high temperature. The answer to this question is of possible relevance to electroweak baryogenesis. It is well known that this does not happen in supersymmetric theories because the thermal contributions of bosons and fermions (supersymmetric partners) do not cancel each other. However, the answer is less obvious for theories with same spin partners. In Chapter 2, using the Twin Higgs model as a benchmark, we show that although thermal corrections do cancel at the level of quadratic divergences, subleading corrections still drive the system to a restored phase. We further argue that our conclusions generalize to other well-known extensions of the Standard Model where the Higgs is rendered natural by being the pseudo-Nambu-Goldstone mode of an approximate global symmetry.

1.3 A particle physics model for dark matter

Closely connected to the endeavors of particle physics is the quest to explain the structure of the universe based on the fundamental principles of physics.

As encapsulated in the 'ΛCDM' paradigm, astrophysical observations (see refs. [5, 15] and references therein) indicate that a significant fraction of the energy density in the universe (and the major contribution from matter-like species) belongs to an effectively collisionless component with its only significant effects being mediated by gravity, lending it the name of 'dark matter'. While it is not strictly necessary for this component of energy to be modelable as (elementary) particles, there does seem to be a curious co-incidence linking the properties of dark matter to the electroweak scale, as explained below.

It has been observed that in simple models of dark matter, demanding a match for the observed relic abundance requires the dark matter annihilation cross section to

correspond to a weak-scale process. Dubbed the 'WIMP miracle' where WIMP stands for Weakly Interacting Massive Particle, this result is a consequence of the fact that the weak scale is located roughly mid-way, geometrically, between the Planck scale and the temperature at the epoch of matter-radiation equality. With this motivation, a large fraction of models proposed have attempted to tie together dark matter models with physics of the SM electroweak sector, most often with solutions to the hierarchy problem. Depending on the details, the mass of dark matter particles is also typically around the weak scale, in this paradigm.

Since the relic abundance is set by the annihilation cross-section, models in this paradigm specify a typical scale for the indirect detection signals expected to be observed. Further, under certain assumptions, the same models could be effectively probed through direct detection and particle colliders as well.

However popular the WIMP paradigm, lack of experimental evidence favoring it behooves us to consider other guiding principles to construct models for dark matter. A curious and unexplained coincidence is that the abundance of dark matter in the universe is the same order of magnitude as baryonic matter. This could be a natural outcome if the dark matter relic were set in the same fashion, and at the same time, as the Standard Model baryonic asymmetry. This is a motivation for considering models with 'Asymmetry Dark Matter' (ADM) (see refs. [16–23]). In this paradigm, the dark matter relic would be dominated by particles, rather than an equal split among particles and anti-particles. Since these particles can hardly find any counterparts to annihilate with, today, such models might be resistant to being probed through indirect detection.

In Chapter 3 we study a mechanism where the dark matter number density today arises from asymmetries generated in the dark sector in the early universe, even

though total dark matter number remains zero throughout the history of the universe. The dark matter population today can be completely symmetric, with annihilation rates above those expected from thermal WIMPs. We give a simple example of this mechanism using a benchmark model of flavored dark matter. We also discuss the experimental signatures of this setup, which arise mainly from the sector that annihilates the symmetric component of dark matter.

Chapter Two: Can A Pseudo-Nambu-Goldstone Higgs Lead To Symmetry Non-Restoration?[1]

Naturalness of the Standard Model (SM) requires the cancellation of divergent contributions to the Higgs mass at the loop level. Most known solutions of the little hierarchy problem involve introducing new particles that cancel the divergences caused by their SM partners, where the cancellation relies on the existence of a symmetry. In the case of supersymmetry (SUSY) the symmetry in question is a spacetime symmetry that relates bosons and fermions whereas models that realize the Higgs field as a pseudo-Nambu-Goldstone boson (pNGB) accomplish this with an internal symmetry. To be precise, in this chapter we will assign a very specific meaning to the word "natural", namely we will label a model as natural if (after cancellations) any existing quadratically divergent contributions to the Higgs potential are of the same order as, or negligible to the leading logarithmic contributions.

In the SM, electroweak symmetry is restored at temperatures above $\mathcal{O}(100)$ GeV [25–30]. Extensions of the SM display a similar behavior at finite temperature. In particular, finite temperature breaks SUSY, and therefore the diagrams whose quadratic divergences cancel each other at zero temperature no longer cancel at finite temperature, generating a thermal mass for the Higgs proportional to T^2 and restoring electroweak symmetry. On the other hand, there is no a priori reason why the cancellation of quadratic divergences should not persist at finite temperature for models with same-spin partners. It was investigated in ref. [31–33] whether this may lead

[1]This chapter is based on work previously published as ref. [24]. This author contributed to the goals and methodology, performed calculations, and contributed to the text and figures in the publication.

to the existence of a broken phase of electroweak symmetry at high temperature in Little Higgs models [34–38][2]. In the following, we will perform a similar analysis on a theory with same-spin partners.

A calculation keeping only the quadratically divergent but not subleading contributions to the Higgs finite temperature effective potential can be justified when SM partners thermally populate the plasma, which happens only close to the cutoff of the effective field theory. However, in theories such as the Littlest Higgs [38] where the Higgs is nonlinearly realized as a pNGB, higher dimensional terms in the effective potential can become important close to the cutoff due to power-law divergent contributions. Then, a one-loop analysis may prove insufficient for calculations at energies above the decay constant f of the sigma model. In fact, the effective field theory of the Littlest Higgs nonlinear sigma model becomes strongly coupled well below $4\pi f$ due to higher-dimensional operators being corrected by scalar loops [42]. Thus, the analysis in ref. [31] with the Littlest Higgs EFT is untrustworthy for $T \gtrsim f$ since Matsubara modes have masses of order πT. For this reason, we will choose a benchmark model in this chapter which has a weakly coupled linear UV completion, namely the Twin Higgs [43], where a one-loop calculation should be reliable.

In our calculation, we will include subleading corrections in the finite temperature potential, which are of a size comparable to the zero-temperature effective potential, and therefore cannot be neglected. We find that while we agree with ref. [31] that the thermal corrections of $\mathrm{O}\left(T^2\right)$ do cancel, subleading corrections still restore the symmetry at high temperature in the Twin Higgs model. Furthermore, we will argue that our conclusions extend beyond the Twin Higgs model, and should remain valid in models where the cancellation of $\mathrm{O}\left(T^2\right)$ corrections to the Higgs potential are

[2]Of course, the subject of possible symmetry non-restoration has a long history that significantly predates the Little Higgs mechanism, starting with refs. [39–41].

ensured by an approximate global symmetry of which the Higgs is a pNGB, and therefore electroweak symmetry is generically restored at high temperature in models that are natural according to our definition.

This chapter is organized as follows: We review the salient features of the Twin Higgs model in section 2.1, followed by a review of the general aspects of calculating the finite temperature effective potential in section 2.2. We then calculate the finite temperature effective potential for our benchmark model and we present the results in section 2.3. In section 2.4 we consider the symmetry structure of other well-known natural extensions of the SM where the Higgs is realized as a pNGB and we conclude that the lessons learned from the benchmark model are generic.

2.1 The Twin Higgs model

There are several variations keeping with the spirit of the Twin Higgs setup [43–53] and here we adopt a minimal version of the model presented in ref. [53] as a benchmark model, and limit ourselves to a description of the aspects most relevant to our purposes. The reader is invited to consult the original references for any additional details not presented here.

In very rough terms, Twin Higgs models introduce a second set of degrees of freedom identical to the SM. The second set of fermion fields fill out the same gauge representations under the new gauge groups as the SM fermions do under the SM gauge groups. The two sectors couple to each other through the scalars (Higgs), and in our benchmark model, they are both charged under $U(1)_Y$. Furthermore, an approximate $\mathbb{Z}_2$ symmetry relates these two sectors (with sector A being identified as the SM). Since the main interest in constructing the Twin Higgs setup is to keep contributions to the Higgs potential under control, in many phenomenological studies,

all fermion fields are neglected, for simplicity, except those that are relevant for cancelling the divergent contributions due to the top Yukawa coupling, and this is the approach that we adopt as well.

For the purposes of this study, we will take the gauge symmetry of the theory to be

$$G = [SU(3) \times SU(2)]^2 \times U(1)_Y \equiv [SU(3) \times SU(2)]_A \times [SU(3) \times SU(2)]_B \times U(1)_Y, \tag{2.1}$$

and the relevant fermionic degrees of freedom in the top sector fill out the representations $Q_{A,B} = (3,2)_{A,B}$, $T^c_{A,B} = (\bar{3},1)_{A,B}$ with hypercharges $1/6$ and $-2/3$, respectively. Under the $\mathbb{Z}_2$ symmetry, the gauge and matter fields of the A and B sectors are exchanged (and the $U(1)_Y$ is unaffected).

It should be noted that this choice of the gauge sector is not phenomenologically viable. In particular since there is only one $U(1)$ factor, the heavy Z' particle inherits couplings to the SM fermions that are experimentally excluded. Adding a second $U(1)$ factor without additional model building in the exact $\mathbb{Z}_2$ limit is also problematic, since it leads to the existence of a second massless photon. A number of phenomenological studies of the Twin Higgs model and its variants have focused on these and other issues [54–93] however for the purposes of this chapter we choose to work with this very minimal model. While extended models exist that address such phenomenological issues, using such a model would only obscure the simple idea behind our analysis without significantly altering our conclusions [3].

The cancellations to the Higgs mass arise from an approximate $SU(4)$ global symmetry in the scalar sector, of which the $SU(2)_A \times SU(2)_B$ subgroup is gauged.

[3]Most extended models need to introduce additional breaking of the $\mathbb{Z}_2$ symmetry, and deviations from the exact symmetry limit tend to reintroduce quadratic divergences which lead to $\mathrm{O}\left(T^2\right)$ symmetry restoring mass terms.

The scalar degrees of freedom belong to the fundamental representation of this global $SU(4)$ symmetry, such that under the gauged subgroup they transform as

$$H \equiv \begin{bmatrix} H_A \\ H_B \end{bmatrix} \longrightarrow \left[\begin{array}{c|c} SU(2)_A & \\ \hline & SU(2)_B \end{array}\right] \begin{bmatrix} H_A \\ H_B \end{bmatrix}. \tag{2.2}$$

Up to a term that will be added later, the tree level potential for the scalars is chosen to respect the global $SU(4)$ symmetry,

$$V(H) = \frac{\lambda}{4}\left(|H|^2 - f^2\right)^2. \tag{2.3}$$

The $SU(4)$ symmetry is spontaneously broken down to $SU(3)$ as H acquires a vacuum expectation value (VEV), which results in seven Nambu-Goldstone bosons and a heavy radial mode. Below the scale f, the radial mode can be integrated out to obtain a nonlinear sigma model for the degrees of freedom parameterized as

$$\exp\frac{i}{f}\left[\begin{array}{ccc|c} & & & h_1 \\ & 0 & & h_2 \\ & & & h_3 \\ \hline h_1^* & h_2^* & h_3^* & h_0 \end{array}\right] \begin{bmatrix} 0 \\ 0 \\ 0 \\ f \end{bmatrix} \equiv \begin{bmatrix} if\frac{h}{\sqrt{h^\dagger h}}\sin\left(\frac{\sqrt{h^\dagger h}}{f}\right) \\ if\frac{h'}{\sqrt{h'^\dagger h'}}\cos\left(\frac{\sqrt{h^\dagger h}}{f}\right) \end{bmatrix}, \tag{2.4}$$

which defines h as the SM Higgs doublet field, and h' as the twin Higgs which is charged under the twin $SU(2)$. It is straightforward to see that to leading order, $h = H_A$.

The global $SU(4)$ is broken down to $SU(2)_A \times SU(2)_B$ when the theory is gauged, and once the Yukawa interactions are introduced, where H_A couples Q_A and T_A^c, and H_B couples Q_B and T_B^c.

$$\mathcal{L}_{\text{Yukawa}} = y\left(H_A^\dagger Q_A T_A^c + H_B^\dagger Q_B T_B^c\right) \tag{2.5}$$

Note that these terms are compatible with the $\mathbb{Z}_2$ symmetry even though they explicitly break the $SU(4)$. This has a very important consequence: one-loop corrections to

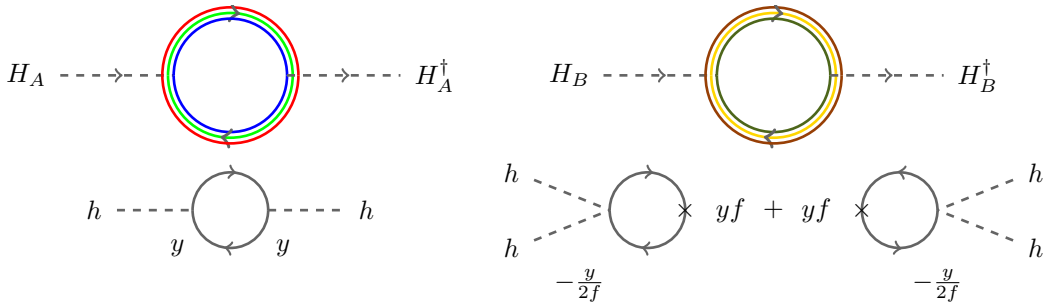

Figure 2.1: The cancellation of quadratic divergences in the top sector in terms of Feynman diagrams in the linear (top row) and non-linear (bottom row) formulations of the model.

the quadratic part of the scalar potential respect the $\mathbb{Z}_2$, that is, they are proportional to $H_A^\dagger H_A + H_B^\dagger H_B$, which can be written as $H^\dagger H$ [4]. In other words, leading quantum corrections to the quadratic part of the potential accidentally respect the full global $SU(4)$ symmetry. Specifically, corrections from the Yukawas and the $SU(2)$ gauge groups have the following form:

$$V_1(H) \supset \left[-\frac{3y^2\Lambda^2}{8\pi^2} + \frac{9g^2\Lambda^2}{64\pi^2}\right]\left(H_A^\dagger H_A + H_B^\dagger H_B\right). \tag{2.6}$$

Therefore, any quadratically divergent contributions give a mass to the radial mode of $H^\dagger H$, but not the SM Higgs doublet h. This cancellation is easiest to see from the linear theory, and appears to be somewhat mysterious from the point of view of the low energy theory due to an unusual four-point coupling between the SM Higgs doublet and the partner fermions. This is illustrated in figure 2.1. The $\mathbb{Z}_2$ similarly prevents divergent contributions from the gauge sector, which again is most easily seen in the linear theory, but of course this also holds true in the nonlinear sigma model of the low energy theory after the radial mode has been integrated out.

[4] In fact, quadratically divergent mass corrections have this property to all loop orders. Even if the Z_2 symmetry is softly broken by the μ^2 term to be introduced later in this section, there will be higher-loop mass corrections proportional to μ^2 but those are not quadratically divergent.

More quantitatively, the one-loop Coleman-Weinberg potential (in Landau gauge)

$$V_{CW}(H) = \frac{1}{64\pi^2}\mathrm{STr}\left[m^4(H)\left(\log\left(\frac{m^2(H)}{\Lambda^2}\right) - \frac{3}{2}\right)\right] \tag{2.7}$$

includes contributions from the top sector, where

$$m^2_{t_A} = y^2 f^2 \sin^2\left(\frac{v}{\sqrt{2}f}\right) \quad \text{and} \quad m^2_{t_B} = y^2 f^2 \cos^2\left(\frac{v}{\sqrt{2}f}\right), \tag{2.8}$$

with $\langle h\rangle = \frac{1}{\sqrt{2}}(v, 0)$, and from the gauge sector, where, in the $g_{U(1)_Y} \to 0$ limit

$$m^2_{W_A} = \frac{g^2 f^2}{2}\sin^2\left(\frac{v}{\sqrt{2}f}\right) \equiv \frac{g^2 v^2_{\mathrm{EW}}}{4} \quad \text{and} \quad m^2_{W_B} = \frac{g^2 f^2}{2}\cos^2\left(\frac{v}{\sqrt{2}f}\right) \tag{2.9}$$

Since the tree level potential thus far respects the $SU(4)$ symmetry, no potential for h is generated from the scalar sector at one loop. Thus h only acquires a mass at one-loop through the top and gauge sectors, with the former dominating over the latter.

The scale of electroweak symmetry breaking v_{EW} is defined in terms of the gauge boson masses, as shown in eq. (2.9). Since the Higgs particle is among the non-linearly parameterized Goldstone modes, $\sqrt{2}\langle h\rangle = v \neq v_{EW} = 246$ GeV (see figure 2.2). As discussed in ref. [83], this implies that the coupling of the Higgs to the weak bosons would deviate from the SM predicted values by a factor of $\cos\left(\frac{v}{\sqrt{2}f}\right)$. Exact $\mathbb{Z}_2$ symmetry implies $v_{\mathrm{EW}} = f$ and that the Higgs couples with equal strength to both A and B sector gauge bosons. For this reason, exact $\mathbb{Z}_2$ symmetry is not phenomenologically viable.

If we assume that the exact $\mathbb{Z}_2$ is broken such that $v_{\mathrm{EW}} \ll f$, with the partner sector being heavier than the SM, the mass of the Higgs is set roughly as

$$m^2_h \sim \frac{3y^2}{8\pi^2} m^2_{t_B} \log\left(\frac{\Lambda^2}{m^2_{t_B}}\right) \sim \left(\frac{f}{\pi}\right)^2, \tag{2.10}$$

So, for $m_h = 125$ GeV, we are led to expect $f \sim 500$ GeV, which also justifies the assumption of $\mathbb{Z}_2$ breaking. For more details on phenomenological considerations in Twin Higgs models and experimental consequences, see ref. [54–93]

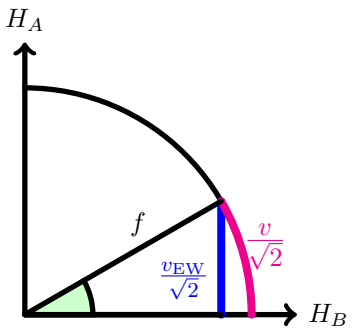

Figure 2.2: Graphical illustration of parameters in field space: f and $v \neq v_{\rm EW}$.

To achieve a soft breaking of the $\mathbb{Z}_2$ symmetry, a term $\mu^2 H_A^\dagger H_A$ is added to the potential. Note that having a small μ^2 is technically natural since it is the only coupling in the theory that violates the $\mathbb{Z}_2$ symmetry. So, for $\mu^2 \sim m_h^2$ (which itself arises at one-loop), higher-loop effects of μ^2 can be safely neglected.

2.2 The Effective Potential at finite temperature

In this section we review the basic aspects of finite temperature field theory, which we need to compute the effective potential for the Twin Higgs model in the finite temperature equilibrium state. We use the Matsubara formalism for finite temperature calculations [94, 95].

Let us consider a renormalizable field theory in the perturbative regime, where we only turn on a background value for one scalar degree of freedom, denoted from here on as ϕ. Since we are interested in the phase structure of a gauge theory in particular, the scalar in question will be taken to transform nontrivially under a gauge group. The full one-loop finite temperature effective potential for ϕ can be split up into a

zero temperature part (including one loop effects) and a finite temperature correction

$$V_{\rm eff}(\phi, T) \equiv V_{\rm tree}(\phi) + V_1^{T=0}(\phi) + \Delta V_1^T(\phi, T) \tag{2.11}$$

with

$$\Delta V_1^T(\phi, T) \equiv \frac{T^4}{2\pi^2} \mathrm{STr}\left[J_{b/f}\left(\frac{m_i^2(\phi)}{T^2}\right)\right] \tag{2.12}$$

where for each particle denoted by the label i, $m_i(\phi)$ denotes its mass in the background ϕ, and by our assumption of perturbativity $m_i(\phi) \lesssim \mathrm{O}(\phi)$. The supertrace includes the correct factor accounting for the number of degrees of freedom associated with each particle and a minus sign for fermions. J_b and J_f arise from the Bose-Einstein and the Fermi-Dirac distribution functions respectively, and they are given as functions of $x_i \equiv \frac{m_i^2(\phi)}{T^2}$ as

$$J_b(x_i) = \int_0^\infty dt\, t^2 \log\left[1 - e^{-\sqrt{x_i + t^2}}\right] \tag{2.13a}$$

$$J_f(x_i) = \int_0^\infty dt\, t^2 \log\left[1 + e^{-\sqrt{x_i + t^2}}\right]. \tag{2.13b}$$

Note that due to the gauge symmetry, any phase of ϕ is equivalent, and from this point on we will restrict ourselves to $\phi \geq 0$.

While the effective potential is not a gauge invariant object, the value of the potential in the vacuum state is well-defined [96–98]. Since we are only interested in the question of whether the symmetry is broken, rather than the details of the phase transition, we can simply investigate whether the global minimum of the finite temperature effective potential occurs at the origin of field space, defined as the point where the gauge bosons are massless[5].

For any given value of ϕ, we will mainly be interested in high temperatures $T^2 > \phi^2$ which due to perturbativity is equivalent to $T^2 > m_i^2(\phi)$ as mentioned above, and we

[5]To be precise, the point where the transverse polarizations of the gauge bosons are massless, at the perturbative level.

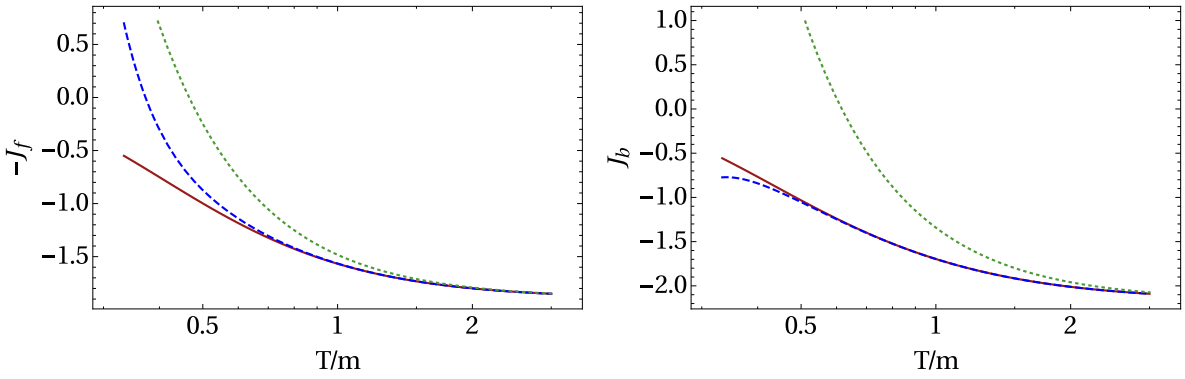

Figure 2.3: Comparison of different truncations of the high temperature effective potential: fermions to the left and bosons to the right. Solid (red) lines represent the numerical evaluation of eq. (2.13), dotted (green) lines and dashed (blue) lines respectively represent truncations to linear order in x and a truncation up to and including the logarithmic terms, in eq. (2.14).

will often drop the subscript to write $x < 1$ to denote the high temperature regime. In this limit the formulae above can be expanded in an asymptotic series (henceforth referred to as the high-temperature expansion)

$$J_b(x) = -\frac{\pi^4}{45} + \frac{\pi^2}{12}x - \frac{\pi x^{\frac{3}{2}}}{6} - \frac{x^2}{32}\log\left(\frac{x}{a_b}\right) + \dots \tag{2.14a}$$

$$-J_f(x) = -\frac{7\pi^4}{360} + \frac{\pi^2}{24}x + \frac{x^2}{32}\log\left(\frac{x}{a_f}\right) + \dots \tag{2.14b}$$

where $a_f = \pi^2 e^{-2\gamma_E + \frac{3}{2}}$ and $a_b = 16\pi^2 e^{-2\gamma_E + \frac{3}{2}}$.

In figure 2.3 we compare, for bosons and fermions respectively, a numerical evaluation of equations (2.13) to the truncation of equations (2.14) at linear order for x, and to a truncation up to and including the logarithmic terms. Inspecting the figure, it is evident that the $\mathrm{O}(x)$ truncation captures the one-loop effective potential only at very high temperatures ($T \gg m$), while the $\log(x)$ truncation does so at roughly $T \gtrsim m$ or even slightly lower temperatures.

Let us consider the salient features of the high-temperature expansion in equation (2.14) term by term, starting with the largest thermal contributions.

Terms of $\mathrm{O}\,(x^0)$: Both bosons and fermions have ϕ-independent Stefan-Boltzmann contributions $\sim T^4$. This does not affect the structure of symmetry breaking.

Terms of $\mathrm{O}\,(x^1)$: This is the first order at which V_{eff} picks up a ϕ dependence, and since $T^4\,x = T^2 m_i^2(\phi) \sim g^2 T^2 \phi^2$ where g symbolically denotes the strength of coupling between ϕ and the particle labeled by the index i, the contributions of $\mathrm{O}\,(x)$ provide an effective thermal mass for ϕ proportional to gT (masses in the EFT are parametrically smaller than the Matsubara scale πT). At finite temperature, bosonic and fermionic modes running in a loop contribute to this term with the same sign because they have opposite boundary conditions on the thermal circle. This is connected to the fact that supersymmetry is broken at finite temperature, and the scalar mass term can acquire large positive corrections $\delta m_{\text{th}}^2 \sim g^2 T^2$ in a supersymmetric theory even though contributions to m^2 cancel at zero temperature. These contributions to the effective thermal mass of ϕ generically drive the scalar background value towards the origin of field space. For bosons and fermions respectively, one can set up a correspondence between thermal mass corrections and zero temperature divergent mass contributions [99]

$$\text{bosons:} \quad \frac{\Lambda^2}{16\pi^2} \longrightarrow \frac{T^2}{12} \tag{2.15a}$$

$$\text{fermions:} \quad -\frac{\Lambda^2}{16\pi^2} \longrightarrow \frac{T^2}{24}. \tag{2.15b}$$

On the other hand, a symmetry that leads to cancellations between the contributions of same-spin particles to the mass of ϕ at zero temperature will also induce a cancellation among corresponding thermal mass contributions, which makes symmetry non-restoration at finite temperature a possibility. This is precisely the case in models where the Higgs is embedded as a pNGB in a nonlinear sigma model and the coupling of the Higgs to the heavy fermionic partners arises from higher dimensional

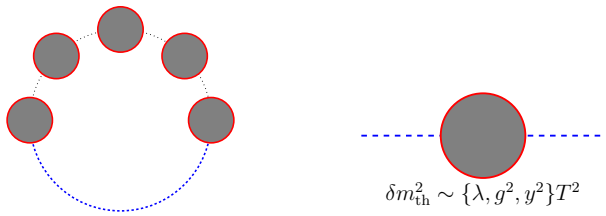

Figure 2.4: Schematic diagram of daisy resummation. Blue (dashed) lines correspond to zero-modes and the blobs correspond to the loops involving higher Matsubara modes.

terms. This is how the divergences can conspire to cancel at zero temperature, as illustrated in figure 2.1. This cancellation can be preserved when the model is UV-completed into a linear sigma model, which is true in the linear formulation of the Twin Higgs model presented in section 2.1.

If the $\mathrm{O}\left(x\right)$ terms can be made to cancel in this fashion, then the phase structure of the model will depend on the effect of the subleading terms in equation (2.14) which therefore must not be neglected. The physics behind these terms is more subtle and we discuss them next.

Terms of $\mathrm{O}\left(x^{3/2}\right)$: In the Matsubara formalism one can expand the fields into their Kaluza-Klein modes around the compact thermal direction. All heavy modes can then be integrated out, leaving us with a dimensionally reduced effective field theory (EFT) of the zero modes, in three (spatial) dimensions. Note that due to their boundary conditions, fermionic degrees of freedom do not have zero modes and therefore the EFT is a theory of scalars and gauge bosons only. As can be seen in temporal gauge, the gauge boson degrees of freedom arrange themselves into an adjoint scalar $\langle A_\tau \rangle$ and a gauge field A_i. By dimensional analysis in this EFT, corrections to the vacuum energy from zero modes running in loops must be proportional to $m^3(\phi)$, which is nothing but the $x^{3/2}$ term in equation (2.14).

Massless zero modes running in loops lead to infrared divergences at higher loop order, which means that a one-loop calculation is inadequate close to the phase transition. A better way to deal with the zero modes is to include the $\mathrm{O}(x)$ thermal corrections to their masses discussed above and use the full thermal mass $m^2_{\rm th}(\phi,T) = m^2(\phi) + \delta m^2_{\rm th}(T)$ when calculating their contribution to the one-loop effective potential [6]. This is equivalent to resumming a series of higher-loop diagrams known as "ring diagrams" or "daisies" (illustrated in figure 2.4) that capture the most egregious infrared divergences, and it is particularly important at temperatures where the thermal mass correction is comparable to, or larger than $m^2(\phi)$. The ring-corrected finite temperature effective potential thus becomes

$$V_{\rm eff}(\phi,T) \equiv V_{\rm tree}(\phi) + V_1^{T=0}(\phi) + \Delta V_1^T(\phi,T) + \Delta V_{\rm ring}(\phi,T), \tag{2.16}$$

with

$$\Delta V_{\rm ring} = \sum \frac{T^4}{12\pi}\left[\left(\frac{m^2(\phi)}{T^2}\right)^{\frac{3}{2}} - \left(\frac{m^2(\phi)+\delta m^2_{\rm th}(T)}{T^2}\right)^{\frac{3}{2}}\right]. \tag{2.17}$$

where the summation runs over all the scalar degrees of freedom in the dimensionally reduced EFT.

At high enough temperatures $m^2_{\rm th}(\phi,T)$ becomes positive, even for scalars which have $m^2(\phi) < 0$ at zero temperature. This eliminates contributions to the effective potential coming from the $x^{3/2}$ term that naively appear to be imaginary [101]. Note that in the Twin Higgs model all scalar modes are pNGBs of the $SU(4)$ symmetry at tree level and therefore do not contribute to the one-loop potential for the SM Higgs which is also among the pNGBs, so this particular issue does not arise.

For zero modes of the transverse polarizations of gauge bosons, residual gauge symmetry in the dimensionally reduced EFT prevents any perturbative mass correc-

[6] As shown in ref. [100] $\langle A_\tau \rangle$ acquires a positive mass, which allows us to restrict our attention to only the 4d scalars as the order parameter for the phase transition.

tions, including ring diagrams. However, the gauge coupling in the 3d EFT has dimensions of mass, which leads to a non-perturbative mass correction $\delta m^2_{\rm np} \sim g^4 T^2$ [102]. Lattice results [103] indicate that such non-perturbative corrections cannot be neglected in the case of the SM, since they affect the nature of the phase transition and reveal the correct expansion parameter of any perturbative description to be $\frac{m_h^2}{m_{\rm W}^2}$.

Even using the best analytical methods available, studying the phase transition is a hard problem [104]. This should not be surprising, since a phase transition corresponds to a non-analyticity in how the free energy depends on the parameters of the model, which cannot be captured at any finite order of perturbation theory [39]. While lattice methods are the most reliable approach in cases such as second order phase transitions, for stronger phase transitions we can gain a qualitative understanding by using analytical methods [105]. We pursue the latter approach here, and hope that our conclusions may serve to motivate further analysis by others.

Taking into account the corrected masses of gauge bosons in the effective theory, their contribution to the effective potential at high temperature has the following form:

$$\begin{aligned}\sum_{\text{polarizations}} T\big[m^2(\phi)+\delta m^2_{\rm th}(T)\big]^{\frac{3}{2}} &\approx \sum_{\text{polarizations}} \zeta^{\frac{3}{2}} T^4 \left[1+\frac{3}{2}\frac{m^2(\phi)}{\zeta T^2}+\dots\right] \\ &= \sum_{\text{polarizations}} \zeta^{\frac{3}{2}} T^4 + \frac{3}{2}\sqrt{\zeta} T^2\; m^2(\phi) + \mathrm{O}\left(T^0\right)\end{aligned} \tag{2.18}$$

where $\delta m^2_{\rm th}(T) = \zeta T^2$ and ζ contains numerical factors and couplings. The T^4 and T^2 terms imply corrections to the Stefan-Boltzmann term and the thermal mass of ϕ respectively, followed by corrections with non-positive powers of T. Strictly speaking, at temperatures where non-perturbative thermal mass corrections to the mass of the transverse polarizations of the gauge bosons dominate mass contributions coming from the Higgs mechanism, the Higgs VEV ceases to be a good order parameter.

If a cancellation among the $\mathrm{O}\left(T^2\right)$ terms in the one-loop effective potential persists in the three dimensional EFT after the resummation, then keeping the subleading terms of $\mathrm{O}\left(\log T\right)$ becomes crucial to any attempt at an (approximate) analytical study of the phase structure of the theory. For the same reasons as in the discussion of the $\mathrm{O}\left(x\right)$ terms, this is indeed the case for the model at hand so we finally turn our attention to this last set of terms.

Terms of $\mathrm{O}\left(\log x\right)$: Note that for each degree of freedom, the logarithmic terms in eq. (2.14) combine with the logarithmic terms in the zero temperature Coleman-Weinberg potential of eq. (2.7) to give a $\log \frac{a_{b/f}\, T^2}{\Lambda^2}$ dependence on the temperature, as the factors of $m^2(\phi)$ cancel between the one-loop corrections at zero and finite temperature. Any formal cutoff dependence thus comes from the zero temperature Coleman-Weinberg potential, whose parameters have been chosen to reproduce the observed electroweak VEV and Higgs mass. As we will see in the next section, the non-cancellation of these terms will determine the fate of electroweak symmetry restoration at finite temperature, in the Twin Higgs model we consider.

Having reviewed the most important aspects of field theory at finite temperature in general, we will apply what we have learned specifically to the Twin Higgs model in the next section.

2.3 Twin Higgs at finite temperature

Let us now specialize our discussion to the Twin Higgs model at finite temperature, and let us consider whether there can be any important contributions to the effective potential that we have not already accounted for in the previous section. Due to invariance under gauge symmetries, $H_A^\dagger H_A$ and $H_B^\dagger H_B$ are the only combinations that the effective potential can depend on at zero or finite temperature, and in the

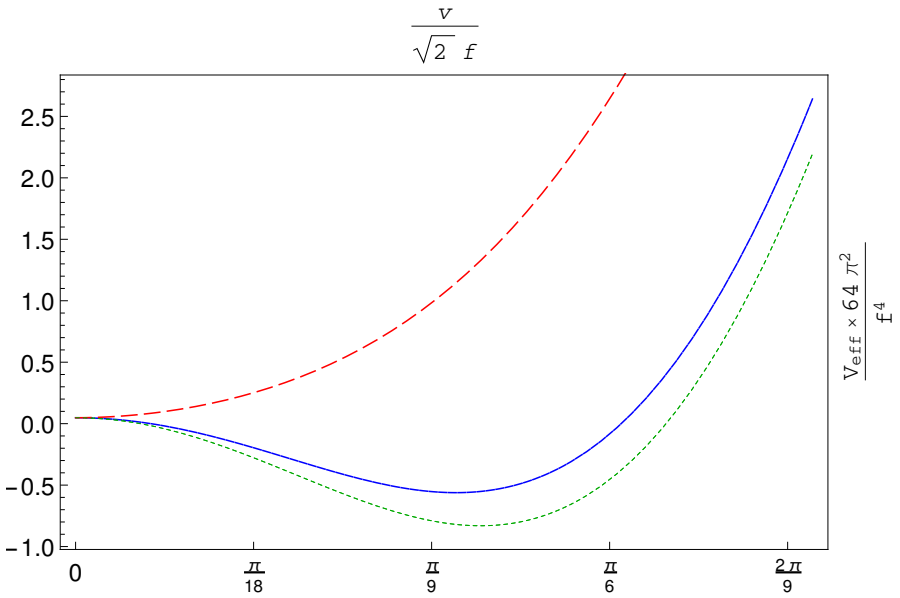

Figure 2.5: We plot the finite temperature effective potential at two different temperatures: The blue solid line represents the potential (numerically evaluated) at $T_1 = 100$ GeV, the red dashed line represents the potential (numerically evaluated) at $T_2 = 350$ GeV and the green dotted line represents the $\mathrm{O}\left(T^2\right)$ truncation of the potential. Note that for the quadratic truncation, the potential is independent of temperature, and hence, does not sense symmetry restoration. See the main text for the numerical values of the relevant parameters that were used in making the plot.

exact $\mathbb{Z}_2$ limit these have identical coefficients, which ensures an accidental $SU(4)$ symmetry for quadratic terms, forbidding any dependence on the Goldstone modes at that order. Furthermore, even though the $\mathbb{Z}_2$ is broken by the μ^2 term introduced at the end of section 2.1, this is a soft breaking, thus any $\mathbb{Z}_2$ violating corrections to the potential must include a positive power of μ^2. This means that by simple dimensional analysis, at the renormalizable level there can be no $\mathbb{Z}_2$ violating contributions to the potential with a positive power of temperature that depend on the Goldstone modes either. There can be contributions of order $\log(T)$ that are $\mathbb{Z}_2$ violating, but these are subdominant to the contributions of order $\log(T)$ that have already been considered at the end of section 2.2, since $\mu^2 \ll f^2$.

Of course, the potential has a dependence on the Goldstone modes beyond quadratic order, where $\mathbb{Z}_2$ invariance is no longer equivalent to full $SU(4)$ invariance, leading to terms such as $\left(H_A^\dagger H_A\right)^2 + \left(H_B^\dagger H_B\right)^2$. Being dimension four operators, by dimensional analysis the coefficients of such terms also cannot include a positive power of temperature, so these fall into the class of contributions of order $\log(T)$ that we have already discussed.

Since we have now convinced ourselves that all thermal mass corrections of $\mathrm{O}\left(T^2\right)$ cancel, let us proceed to evaluate the logarithmic contributions from the top quark and its partner:

$$\begin{aligned} -(3\times 4) & \left[\frac{\left(y^2 f^2 \sin^2\frac{h}{f}\right)^2}{64\pi^2} + \frac{\left(y^2 f^2 \cos^2\frac{h}{f}\right)^2}{64\pi^2}\right]\log\frac{a_F T^2}{\Lambda^2} \\ &= -12\left[\frac{\left(y^2\{h+\ldots\}^2\right)^2}{64\pi^2} + \frac{\left(y^2\left\{f-\frac{h^\dagger h}{2f}+\ldots\right\}^2\right)^2}{64\pi^2}\right]\log\frac{a_F T^2}{\Lambda^2} \\ &\sim \quad \ldots + \frac{3y^4 f^2 h^\dagger h}{8\pi^2}\log\frac{a_F T^2}{\Lambda^2} + \ldots \end{aligned} \tag{2.19}$$

In hindsight, the fact that these subleading contributions do not cancel each other should come as no surprise. The non-cancellation of logarithmic terms between $\mathbb{Z}_2$ partners in the one-loop Coleman-Weinberg potential is precisely what keeps the Higgs from being an exact Goldstone boson and ensures a sizable Higgs mass at zero temperature (see for instance equation (2.10)). As mentioned previously, note that the appearance of Λ eq. 2.19 arises from the zero temperature Coleman-Weinberg potential, and the finite temperature additive corrections are independent of the cutoff (refer eq. 2.14).

More generally, in the case of phenomenologically viable SM extensions with a pNGB based mechanism for naturalness, any ultraviolet divergent contribution to

the Higgs effective potential at zero temperature will carry over to a corresponding finite temperature contribution. In the specific case of the Twin Higgs model, as well as in other natural models with a similar symmetry structure, we expect this feature to drive symmetry restoration at finite temperature.

If we wish to study the phase of the theory at temperatures around the electroweak scale (and not significantly higher than the partner masses), it is straightforward to numerically evaluate the one-loop effective potential. While the high-temperature approximations in eq. (2.14) are analytically tractable and help shape our thinking, we choose to numerically evaluate eq. (2.12) and eq. (2.13) in order to avoid any artifacts from truncating the expansion. The results for our benchmark model (with $f = 450$ GeV, $\mu = 90$ GeV and $\Lambda = 4.4$ TeV) are presented in figure 2.5. The most important one-loop effects come from the top sector, followed by the electroweak gauge sector, resulting in the restoration of electroweak symmetry at $T \sim 300$ GeV (which stays restored as we push temperatures up to where the EFT starts breaking down).

Since non-perturbative effects cloud the study of physics close to the phase transition, it would be nice to attack this question from a different angle. In particular, it would be of interest to look for a symmetry restored phase at temperatures much higher than the phase transition, where a resummed theory has a valid perturbative description. Of course, this cannot be done in the nonlinear Twin Higgs model and necessitates a UV-completion, which we take to be a linear sigma model completion of the Twin Higgs described in section 2.1. In this UV-completion, the "radial mode" linearizes the sigma model. The radial mode is a singlet of the approximate $SU(4)$ global symmetry in the scalar sector, and thus its zero-temperature mass will not be protected from quadratically divergent contributions. This means that at high

temperatures, the radial mode picks up a positive thermal mass term, leading to a symmetry restored phase in the UV completion. The radial mode being driven to zero is a sufficient condition for the gauge bosons to become massless (up to thermal contributions). Note that this result is not directly related to our calculation in the nonlinear model, as the VEVs of the radial mode and the Goldstone modes are separate from each other.

2.4 Conclusions and Outlook

We have investigated the possible existence of a broken phase of electroweak symmetry at high temperature in extensions of the Standard Model where the Higgs is realized as a pNGB, focusing on the Twin Higgs model as a benchmark. While we have confirmed that one-loop quadratic contributions to the Higgs potential at finite temperature cancel between the Standard Model degrees of freedom and their partners as they do at zero temperature, this is not true for subleading corrections to the effective potential, which restore electroweak symmetry at high temperature. Cancellation of $\mathrm{O}\left(T^2\right)$ corrections to terms in the the Higgs potential is a generic consequence of same-spin partners ensuring naturalness at zero temperature, and the logarithmic corrections are connected to obtaining a phenomenologically viable Higgs boson mass at zero temperature. In the case of the Littlest Higgs model considered in ref. [31], the EFT has uncancelled quadratically divergent corrections to higher-order terms in the Higgs potential (arising from non-renormalizable operators), but even in that case, the theory exhibits a restoration of electroweak symmetry as long as temperatures are not pushed beyond the range of validity of the EFT for a finite temperature calculation.

It should be noted that nonlinear sigma models in which the Higgs is a pseudo-

Goldstone generically become strongly coupled at high energies and require UV completion, which brings up the question of whether a suitable UV completion may nevertheless allow for a broken phase of electroweak symmetry to persist at high temperature. As we have demonstrated for the case of the Twin Higgs model, UV completing the theory into a linear sigma model cannot achieve this, since the mass of the radial mode is unprotected from quadratic corrections, which at finite temperature drive the radial mode to the origin of field space and lead to symmetry restoration. One can also contemplate nesting one nonlinear sigma model inside another with a higher symmetry breaking scale, however since the Higgs receives a thermal correction (albeit at the subleading level) in the original nonlinear sigma model, this type of construction will not change the finite temperature behavior.

Alternatively, one can imagine supersymmetrizing the linear sigma model, since supersymmetry is the best understood UV-complete mechanism to protect the mass of a scalar from quadratically divergent corrections. However we know that supersymmetry does not prevent quadratic mass corrections at finite temperature, and therefore the radial mode VEV would still be driven to zero.

Let us also briefly remark on classes of natural extensions of the SM other than supersymmetry and Higgs as a pNGB. Theories with strongly coupled Higgs sectors appear to be disfavored in light of the experimental findings at the LHC, and in any case these typically exhibit symmetry restoration for temperatures above the formation of the condensate. Gauge-Higgs models have been shown to lead to a restored symmetry phase at high temperature [106]. In "Relaxion" models [107], electroweak symmetry is also restored at high temperatures, but this idea is quite recent and it would be interesting to study whether variants of it may have a more subtle finite temperature behavior.

Our conclusions are also consistent with more general considerations based on the thermodynamic behavior of systems at high temperature. In particular, the free energy of a system is given by

$$\mathcal{F} = \mathcal{E} - T\mathcal{S}, \tag{2.20}$$

and therefore, heuristically, at high temperatures, the free energy can be minimized by increasing entropy (corresponding to a symmetric phase) rather than lowering the energy by spontaneous symmetry breakdown [108]. This suggests a robust rule of thumb that symmetries get restored at high temperatures, in the absence of any other thermodynamic variables describing the system that can attain values that are "natural" based on dimensional analysis. We remark in passing that if this last criterion is removed, e.g. when the system has a chemical potential $\mu \sim T$, symmetry non-restoration is possible, see for example refs. [109–112].

Chapter Three: Secretly Asymmetric Dark Matter[1]

Asymmetric dark matter (ADM) [16–23] is motivated by the observation that the dark matter and baryon energy densities today are comparable, so that for dark matter masses of a few GeV, the number densities of the dark and visible sectors are also roughly comparable. The baryon number density today is set by an asymmetry, which suggests that dark matter could also be asymmetric, with the origin of the two asymmetries being related. In order to realize the conventional ADM scenario, a mechanism has to be put in place in order to break $U(1)_\chi$, a symmetry which guarantees conservation of dark matter (DM) number, in much the same way that $U(1)_B$ must be broken in order to generate an asymmetry in the visible sector.

The rest of this chapter will present a model where the dark matter abundance was set by asymmetries, *without* breaking the $U(1)_\chi$ symmetry corresponding to conserved dark matter number. Asymmetries can be generated in the different dark sector states, while keeping the total charge under the $U(1)_\chi$ at zero. If heavier states in the dark sector decay to lighter ones after DM annihilations have frozen out [114, 115], then the final DM population is in fact symmetric, even though its abundance was set by an asymmetry. For this reason we will refer to this mechanism as Secretly Asymmetric Dark Matter (SADM). The idea of repopulating the symmetric component of DM at late times through oscillations has also been explored previously [116–120].

[1]This chapter is based on work previously published as ref. [113]. This author contributed to the goals and methodology, performed or verified calculations, and contributed to the text and some figures in the publication.

The relic abundance of DM in this mechanism is in some ways similar to the abundance of charged stable particles in the Standard Model (SM). Even though the abundances of baryons and leptons are set by an initial asymmetry, the universe is always charge neutral and $U(1)_{\rm EM}$ is never broken. If protons were to decay at late times, the universe could end up with a symmetric population of electrons and positrons which is secretly asymmetric.

3.1 A Model based on Flavored Dark Matter

Flavored dark matter (FDM) models [121–137] have multiple dark matter states by construction, as well as a simple way to connect the DM states with baryons or leptons that allows the transfer of asymmetries between the two sectors. Therefore, the SADM mechanism can be naturally realized in FDM models. In this work we will use a model of lepton flavored dark matter to demonstrate how the proposed mechanism works.

Consider a model where three flavors of SM singlet Dirac fermions $(\chi, \chi^c)_{i=1,2,3}$ interact with the right-handed leptons in the SM via a scalar mediator ϕ. The interaction Lagrangian is given by

$$\mathcal{L}_{\rm LFDM} = \lambda_{ij}\phi\chi_i e_j^c + \text{h.c.} \tag{3.1}$$

We will denote the mass of the lightest χ by m_χ and the typical mass splitting between the χ flavors by δm.

It is worth commenting on the conserved quantum numbers in the presence of the interaction in equation 3.1.

- $\tilde{L}_i$ **number**: Individual lepton asymmetries L_i in the SM can be extended by assigning appropriate charges to dark matter flavors χ_i. Then, $U(1)_{B-\tilde{L}}$

remains unbroken and anomaly-free, except the explicit breaking from heavy right-handed neutrinos. If the coupling matrix λ_{ij} is flavor diagonal in the charged lepton and χ mass basis, then the $U(1)_L^3$ flavor symmetry is preserved to a good approximation at low energies–broken only by the mixing among light neutrinos. The neutrino masses are small enough to have no effect on the physics to be discussed here, and will therefore be neglected from here on. The presence of off-diagonal entries in the couplings λ_{ij} do have interesting phenomenological consequences; however for the sake of simplicity we will defer the discussion of these effects to a more detailed study and we will restrict ourselves to the flavor-universal case with $\lambda_{ij} \equiv \delta_{ij}\lambda$

- χ **number**: There is a separate $U(1)_\chi$ conserved symmetry under which all dark matter particles χ_i have the same charge and the mediator ϕ has the opposite charge.

3.2 Generating the asymmetry

We will assume that high-scale leptogenesis [138] (see refs. [139,140] for a review and comprehensive list of references) generates a net $B - \tilde{L}$ asymmetry in the SM sector through out-of-equilibrium decays of the lightest right handed neutrino N_1—which will then be transferred to baryons and to the dark sector. The comoving quantum numbers

$$\begin{aligned} \tilde{\Delta}_i &= \frac{\left(B/3 - \tilde{L}_i\right)}{s} \\ &\equiv \Delta_i - \Delta Y_{\chi_i} \end{aligned} \tag{3.2}$$

are conserved from the end of leptogenesis down to scales where neutrino oscillations become important. Here s is the entropy density, $Y_{\chi_i} = n_{\chi_i}/s$ are the comoving

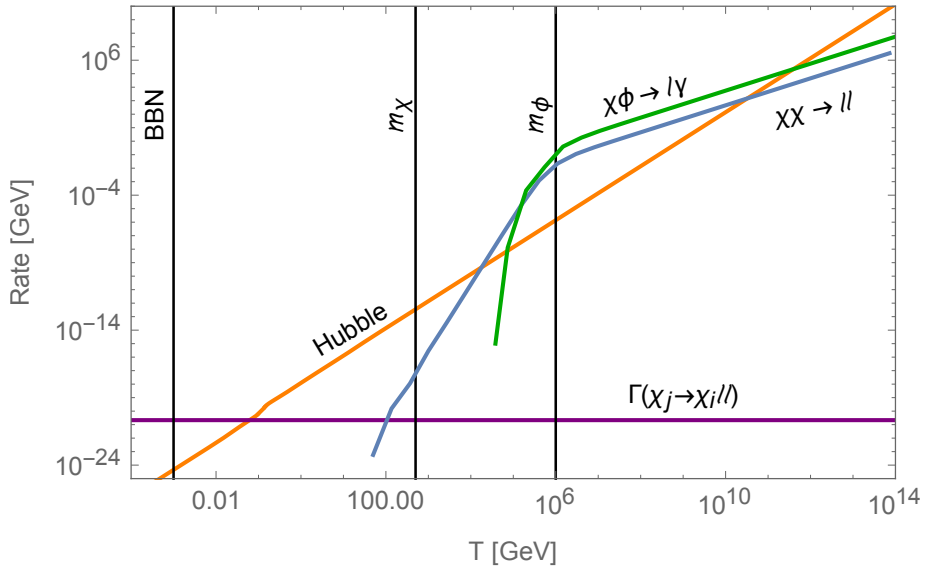

Figure 3.1: Rates of the most important FDM processes and the Hubble scale as a function of temperature for the parameter point defined in the main text.

number densities of dark matter, and $\Delta_i = (B/3 - L_i)/s$ are the conserved comoving quantum numbers in the absence of the dark sector. Depending on which linear superposition of the e, μ and τ flavors N_1 couples to, leptogenesis generates nonzero values for these conserved quantities, which we will take as the initial conditions for the SADM mechanism.

Let us now follow the thermal history of the universe from the end of leptogenesis to lower temperatures. For concreteness we will use a specific parameter point ($\lambda = 0.05, m_\chi = 500$ GeV, $m_\phi = 10^6$ GeV, $\delta m = 0.4 m_\chi$, $T_{\text{leptogenesis}} > 10^{12}$ GeV), and in figure 3.1 we show for this parameter point how the rates of the most important processes in the model compare to the Hubble scale as a function of temperature. With these values, the FDM interaction of equation 3.1 goes into chemical equilibrium after all N have decayed. This is not a necessary condition for the SADM mechanism to work and merely simplifies the discussion, as it lets us take initial conditions

from leptogenesis (values of Δ_i, denoted henceforth as Δ_i^0) in a modular fashion. If the FDM interaction is already in equilibrium during leptogenesis one can solve the Boltzmann equation to track the asymmetries in the two sectors as a function of time.

As the universe continues to cool down, the asymmetry originally generated in the left-handed leptons is transferred to the right-handed leptons (through the SM Yukawas), the baryons (through sphalerons) and to the χ_i (through the FDM interactions). With all these interactions in equilibrium, the comoving asymmetries of all species can be related to the conserved quantities during this epoch (the $\tilde{\Delta}_i$) through equilibrium thermodynamics, with the constraints that the total hypercharge and the total $U(1)_\chi$ number of the universe stay zero. Since individual χ numbers are all zero until the FDM interaction goes into equilibrium, the value of $\left(\tilde{\Delta}_i\right)$ just after is equal to the value of $(\Delta_i) - (\Delta Y_{\chi_i})$ just before, namely Δ_i^0.

At our parameter point, the next step in the thermal evolution is the FDM interaction falling out of equilibrium as the temperature drops below m_ϕ. This decouples the SM and FDM sector asymmetries. Now the comoving asymmetries ΔY_{χ_i} are all separately conserved, and their values are given in terms of the initial conditions as

$$\begin{pmatrix} \Delta Y_{\chi_e} \\ \Delta Y_{\chi_\mu} \\ \Delta Y_{\chi_\tau} \end{pmatrix} = \frac{2}{15} \begin{pmatrix} -2 & 1 & 1 \\ 1 & -2 & 1 \\ 1 & 1 & -2 \end{pmatrix} \begin{pmatrix} \Delta_e^0 \\ \Delta_\mu^0 \\ \Delta_\tau^0 \end{pmatrix}. \tag{3.3}$$

At the same time, the total $B - \tilde{L}$ comoving asymmetry in the SM sector at early times can be related to the baryon number density B_0 and entropy density s_0 today,

$$\Delta Y_{B-\tilde{L}} = \sum_i \Delta_i^0 \approx \frac{79}{28} \frac{B_0}{s_0}, \tag{3.4}$$

which imposes a constraint on the possible initial conditions. From this point on, the thermal evolution of the SM sector proceeds as usual.

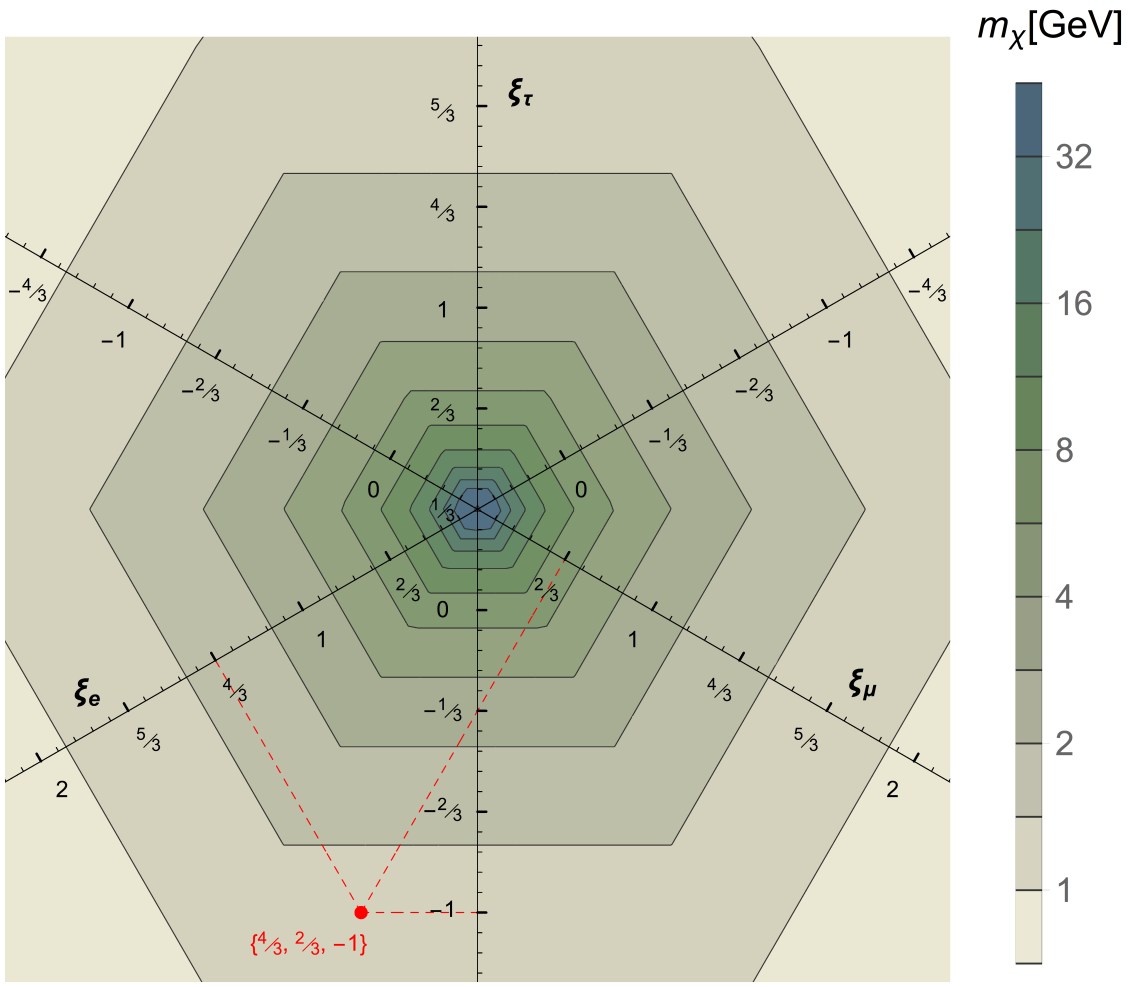

Figure 3.2: The values of m_χ needed to obtain the correct ρ_B and ρ_{DM} as the initial lepton asymmetries Δ_i^0 are varied subject to the constraint of equation 3.4, assuming there is no symmetric component to the relic. The values of $\xi_i \equiv \Delta_i^0/\Delta Y_{B-L}$ for any point can be read off by drawing perpendiculars to the three axes shown.

After the symmetric component of DM annihilates away (through mechanisms discussed below), the DM relic abundance today is given by

$$\rho_{DM} = m_\chi \; s_0 \left(|\Delta Y_{\chi_e}| + |\Delta Y_{\chi_\mu}| + |\Delta Y_{\chi_\tau}| \right). \tag{3.5}$$

Therefore, the ratio

$$\frac{\rho_B}{\rho_{DM}} = \frac{m_p}{m_\chi} \; \frac{28/79 \left(\Delta_e^0 + \Delta_\mu^0 + \Delta_\tau^0 \right)}{|\Delta Y_{\chi_e}| + |\Delta Y_{\chi_\mu}| + |\Delta Y_{\chi_\tau}|} \tag{3.6}$$

relates the value of m_χ to observed values of ρ_B and ρ_{DM} (with $\rho_B/\rho_{DM} = 0.185$ [5]), given any initial condition Δ_i^0. This is illustrated in figure 3.2. Note that ρ_B and ρ_{DM} depend on different combinations of the initial conditions.

While for generic initial conditions we expect m_χ to be a few GeV, both larger and smaller values are possible in the following two limits: If the leptogenesis mechanism generates almost equal Δ_i^0 then equation 3.3 sets the ΔY_{χ_i} to be small, and therefore the DM mass needs to be large to obtain the right ρ_{DM}. On the other hand, if the leptogenesis mechanism generates large individual asymmetries for the SM lepton flavors that almost cancel [141] (e.g. $\Delta_\tau^0 = -\Delta_\mu^0 \gg \Delta_e^0 \sim \Delta Y_{B-L}$) then the denominator in equation 3.6 is large, and the DM mass needs to be small.

3.3 Decays in the dark sector

If the mass splitting $\delta m_{ij} \equiv m_{\chi_i} - m_{\chi_j}$ is less than $m_{\ell_i} + m_{\ell_j}$, the decays $\chi_i \to \chi_j$+X can only proceed through χ-flavor mixing or through strongly suppressed loop processes [142], and the lifetime can be so long that all three χ can be treated as stable for practical purposes. For larger splittings however, the decay $\chi_i \to \chi_j \ell_i \bar{\ell}_j$ proceeds at tree level, with

$$\Gamma \simeq \frac{\lambda^4 (\delta m_{ij})^5}{480 \pi^3 m_\phi^4}. \tag{3.7}$$

If decays become important before χ-$\bar{\chi}$ annihilations freeze out, then they depopulate the heavier flavors and the dark matter abundance is set by the usual symmetric thermal freeze-out. Therefore, if the relic abundance based on the initial asymmetry is to survive at late times, then decays need to happen after annihilations freeze-out, but before Big-Bang Nucleosynthesis (BBN) in order to avoid early universe constraints. This is a core requirement of our set up. It is straightforward to check that this condition is satisfied at our parameter point. The width of the heavier flavors for these parameters is illustrated by the horizontal line in figure 3.1.

3.4 Annihilation of the symmetric DM component

If FDM annihilations $\chi_i \bar{\chi}_j \to l_i^- l_j^+$ are still active below $T \sim m_\chi$, then they deplete the asymmetry in the dark sector. Therefore, another core requirement for SADM is to ensure that the FDM interaction decouples while χ is relativistic. This also implies that we need additional interactions which can annihilate the symmetric component of DM, without depleting the asymmetry. We consider the setup, referred from here on as the Z'-model, where the $U(1)_\chi$ symmetry is gauged with a coupling g_D, and where the gauge boson Z'_μ acquires a small mass $m_{Z'} < m_\chi$. The Z' couples to the χ_i in a flavor-diagonal fashion and leads to efficient χ_i-$\bar{\chi}_i$ annihilations, such that the symmetric component of DM annihilates away for $g_D \gtrsim g_{\text{WIMP}}$, where g_{WIMP} is the coupling that leads to the correct relic abundance for a thermal relic with the same mass.

Since ϕ carries a unit charge under $U(1)_\chi$ as well as hypercharge, it leads to kinetic

mixing [143, 144] between these groups

$$\mathcal{L}_{\text{mix.}} = -\frac{\epsilon}{2} B^{\mu\nu} Z'_{\mu\nu}, \tag{3.8}$$

where the loop of ϕ generates $\epsilon \sim 10^{-3} - 10^{-4}$ for couplings needed to annihilate the symmetric part. However, other UV contributions to the kinetic mixing can lead to a larger or smaller value of ϵ. The Z' can decay to the light SM fermions through the kinetic mixing.

3.5 Experimental Signatures of the Z'-model

If all flavors of χ are long-lived on cosmological timescales then there are no annihilations happening today and therefore indirect detection experiments are not sensitive to this case. If on the other hand only the lightest flavor survives today, then the DM distribution is symmetric. Since there is only a lower limit on g_D, one can obtain a stronger signal in indirect detection for a given m_χ compared to a WIMP. In particular, the annihilations will take the form $\bar{\chi}\chi \to Z'Z' \to 4f$, where f denotes SM fermions with $m_f < m_{Z'}/2$. Depending on $m_{Z'}$, the leading constraint from indirect detection may arise from positrons [7, 8], photons [6] or CMB measurements of ionization [5]. These constraints were considered in ref. [145–147], and they are shown in the lower plot of figure 3.3.

The Z'-hypercharge mixing also gives rise to a signal in direct detection experiments such as LUX [1, 2], SuperCDMS [3] and CRESST-II [4]. Since tree-level Z-exchange is excluded by orders of magnitude, this translates to a strong constraint on the model parameters. In the upper plot of figure 3.3 we show the bounds in the m_χ-σ_0 plane for a specific choice of $m_{Z'} = m_\chi/2$.

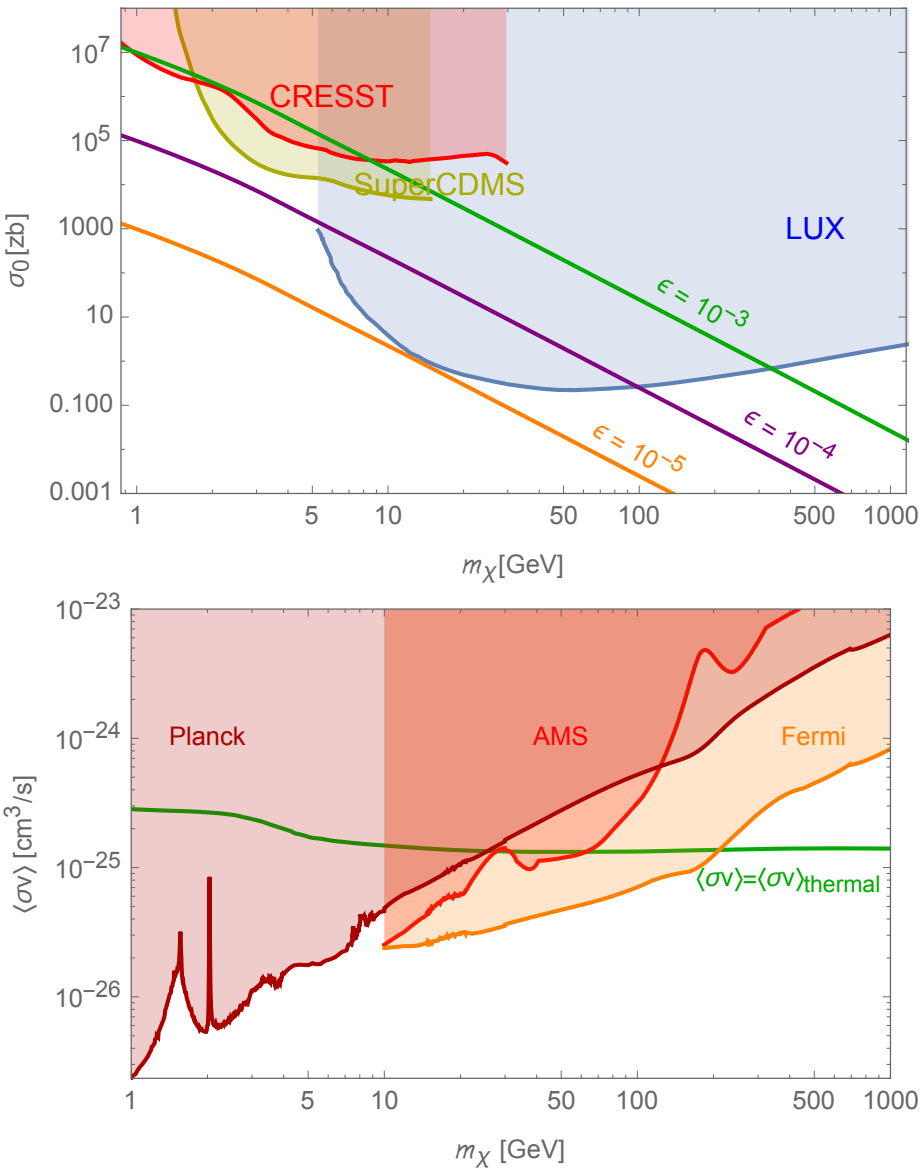

Figure 3.3: Constraints on the Z'-model. *Upper:* Direct detection constraints from LUX [1, 2], SuperCDMS [3] and CRESST-II [4] for representative values of ϵ and $g_D = g_{\text{WIMP}}$. *Lower:* Indirect detection constraints from Planck [5], Fermi [6] and AMS [7, 8]. For reference we also show the annihilation cross section [9] which gives the correct relic abundance in our model with no asymmetry. $m_{Z'}$ is taken to be $m_\chi/2$ for both plots.

Finally, there are also bounds on the model from dark photon searches, which can be quite stringent for a very light Z' [148,149]. However for $m_{Z'} \gtrsim 1$ GeV, the bound for ϵ is typically at the 10^{-3} level, and generic values in our model are compatible with this constraint.

We see that direct detection, indirect detection and dark photon searches provide a complementary set of constraints for the parameter space of the Z' model. Light DM with $m_\chi \simeq 5$ GeV, which can be obtained from generic initial conditions (see figure 3.2), is unconstrained by direct detection even for generic values of ϵ, and can be within reach of future experiments probing light dark matter. The low m_χ region is in tension with indirect detection bounds, but the constraints may be evaded in a modified version of the model, for example if the main annihilation channel is into neutrinos. Heavier $m_\chi \gtrsim O(100\ \text{GeV})$ are unconstrained by either set of bounds.

3.6 Alternative model for annihilating the symmetric part

In order to stress the model dependence of some of the bounds considered above, we describe a variation of the model where DM annihilates via a scalar instead of a Z'. In particular, consider a light real scalar S with the interactions

$$\mathcal{L}_S = \kappa_{ij} S \chi_i \chi_j^c - V(S)\,. \tag{3.9}$$

Consistent with the $U(1)_L^3$ global symmetry we will take $\kappa_{ij} \equiv \delta_{ij}\kappa$. S develops a coupling to the right-handed SM leptons at one loop through the FDM interaction, and can therefore efficiently annihilate the symmetric part of the DM distribution. S does not mix with the Higgs boson until at least the two-loop order, and even

this mixing is suppressed by lepton Yukawa couplings. Therefore, unlike the Z', tree-level S exchange only gives a negligible signal in direct detection experiments. Furthermore, the annihilation channel $\bar{\chi}\chi \to SS$ is p-wave suppressed, which means that even for a fully symmetric χ distribution today, indirect detection signals are expected to be very weak. Thus, this alternative model is basically unconstrained by the experiments discussed above.

3.7 Conclusions

We have studied the SADM mechanism where for a dark sector with multiple states, the relic abundance is set by an asymmetry even though the DM number remains zero. If heavier DM states can decay to the lightest state, then DM is symmetric at late times, whereas otherwise multiple DM components can be present today. This mechanism is realized naturally in models of FDM. Experimental signals, if present, arise mainly due to the sector of the model that is responsible for annihilating the symmetric component of the DM. We have presented two alternatives for this sector: a Z'-model where Z'-hypercharge mixing generically takes place at the one-loop level, and a scalar model where mixing with the Higgs can naturally be very small. For the former model there are a number of experimental constraints from DM searches as well as dark photon searches, and future experiments should be able to probe a sizable fraction of the parameter space currently consistent with constraints. The latter model on the other hand is very difficult to probe experimentally, and its parameter space is largely unconstrained.

Chapter Four: A defect in holographic interpretations of tensor networks[1]

In the last decade, two of the most successful approaches to studying conformal field theories—holographic duality and tensor networks—have turned out to be intimately tied to entanglement. In the context of the AdS/CFT correspondence [151, 152], the Ryu-Takayanagi proposal [153, 154] revealed that holographic spacetimes function as maps of CFT entanglement. Meanwhile, the Multi-scale Entanglement Renormalization Ansatz (MERA) [155,156] arose largely from considering the scale dependence of entanglement entropies in conformal field theories. The fact that quantum entanglement plays a clarifying role in both approaches suggests that holographic spacetimes and MERA networks may be linked by a more direct relationship.

4.0.1 Holography and MERA

A relationship between holography and MERA was first proposed by Swingle [157, 158] (see also refs. [159–163]) who pointed out that the MERA network for a CFT ground state bears a striking resemblance to the geometry of anti-de Sitter (AdS) space. An alternative proposal [164,165] argued that the translation between MERA and holography is mediated by an auxiliary construct termed kinematic space. But both proposals are largely qualitative and would benefit from a broader class of examples, other than the case of the CFT vacuum / pure AdS geometry. Some steps in that direction were taken in refs. [165, 166] (see also refs. [157, 158, 167]) which

[1]This chapter is based on work previously published as ref. [150]. This author contributed to the goals and methodology, performed or verified calculations and contributed to the text and some figures in the publication.

compared MERA representations of CFT_2 thermal states to the BTZ geometries. The analysis in ref. [165] also included Virasoro descendants of the CFT vacuum, related to other locally AdS_3 space-times. One commonality of all these examples is that they rely on the extended conformal symmetry in two dimensions. To further explore how MERA and the holographic duality may come together, we need to consider holographic duals and MERA representations of CFT states, which are not related to the vacuum by the application of an anomalous symmetry.

This is the subject of the present chapter.[2] We consider the ground states of two-dimensional conformal field theories whose global symmetry has been broken from $SO(2,2)$ down to $SO(2,1)$ by the presence of a defect, an interface or a boundary.[3] On the tensor network side, the 'theory of minimal updates' [178] governs the structure of the MERA representations of such states. In holography, there have been many discussions and several explicit examples of holographic defect/interface [179–181] and boundary CFTs [182–184] in two dimensions. Our goal is to compare these MERA networks and holographic geometries and analyze in what way, if at all, they relate to one another.

Our principal findings are the following:

1. In section 4.1, we complement existing arguments [178, 185] which support the validity of the minimally updated MERA and clarify the circumstances under which it is expected to hold. It applies to actual defect and interface CFTs, but not to generic two-dimensional theories with $SO(2,1)$ symmetry.

[2] Other tensor network realizations of broader classes of geometries, mostly set in the context of the ER=EPR [168] and the complexity=action [169] conjectures, include refs. [170–177]. Those works concentrate on the dynamics of space-times while our interest here is on bulk duals of ground states of more general classes of CFTs.

[3] In order not to clutter the text, we will refer to all these setups as 'defects' unless the context requires distinguishing defects, interfaces and boundaries.

2. In section 4.2, we propose **rayed MERA**—a simple generalization of MERA, which should capture ground states of generic two-dimensional theories with $SO(2,1)$ symmetry. In holography, the cases where the minimally updated MERA suffices versus those requiring rayed MERA are distinguished by the boundary region where non-normalizable modes are supported.

3. In section 4.3, we discuss two examples of holographic defect CFTs. We conclude that a naïvely local relation between MERA networks and AdS_3 geometries, in which a specific region of the MERA network corresponds to a specific region of (the spatial slice of) AdS_3, does not hold. This applies both to the direct AdS-MERA correspondence of refs. [157,158] and to the kinematic proposal of refs. [164, 165].

4. Instead, a key ingredient in relating tensor networks to holographic geometries is that every bond should be associated with the amount of entanglement across it and not with more naïve measures such as the bond dimension. This point was already made in ref. [165]; here we exemplify it. We expect this conclusion to apply to all tensor network models of holography, not just to MERA.

Combining these observations leads to the following holographic interpretation of the prescription of ref. [178]: the theory of minimal updates specifies which tensors do / do not register the effect of turning on non-normalizable modes in the bulk. We expand on this statement and put our work in a broader context in the Discussion section.

In the remainder of this section, we briefly recapitulate the notion of kinematic space and MERA. Connections between the two are interspersed through the chapter, as relevant, when we consider different aspects of the proposals relating holography

and MERA. This chapter assumes a familiarity with the AdS/CFT correspondence. A good review of MERA is ref. [186], reviews of AdS/CFT include ref. [187–189] while relevant discussions of parallels between MERA and the holographic duality include refs. [157, 165, 190] (see also ref. [191]). As mentioned previously, throughout this chapter we shall restrict ourselves to two dimensions.

4.0.2 Integral geometry and holography

The fundamental principle of integral geometry is to model a geometry by the set of geodesics on it—what we refer to as kinematic space. The 'Crofton form' refers to the appropriate canonical measure on kinematic space. A calculation of interest, such as finding the length of a curve γ, is carried out by integrating over kinematic space (using the Crofton form ω_K) the number of intersections of any geodesic with γ.

$$\text{length of } \gamma = \frac{1}{4}\int_K \omega_K \; n_\gamma$$

In many simple cases, symmetries of the background geometry constrain the Crofton form up to an overall normalization.

As a warm-up to the calculations needed for the rest of this chapter, we shall illustrate a simple example: an equal-time slice of the Poincaré patch of AdS_2, whose metric is given by

$$ds^2 = L^2 \frac{dz^2 + dx^2}{z^2}$$

Geodesics in this geometry are shaped like semicircles with endpoints on the boundary. Therefore, to compute the Crofton form on kinematic space, we need to consider changes in length of geodesics as both their endpoints are varied slightly. Since the Ryu-Takayanagi formula relates the length of a geodesic to the entanglement entropy of the boundary spatial interval it bounds, a careful consideration (see

ref. [164]) shows that the Crofton form must relate to the mutual information between two infinitesimal regions, conditioned on the interval between them (see figure 4.1), and is given by

$$\omega_K(u,v) \approx S(u-du,v)+S(u,v+dv)-S(u,v)-S(u-du,v+dv) \approx \frac{\partial^2 S(u,v)}{\partial u\,\partial v}\,du\,dv \tag{4.1}$$

The strong sub-additivity inequality (SSA) mandates that this quantity be positive since

$$S(u-du,v)+S(u,v+dv)-S(u,v)-S(u-du,v+dv) \geq 0 \tag{4.2}$$

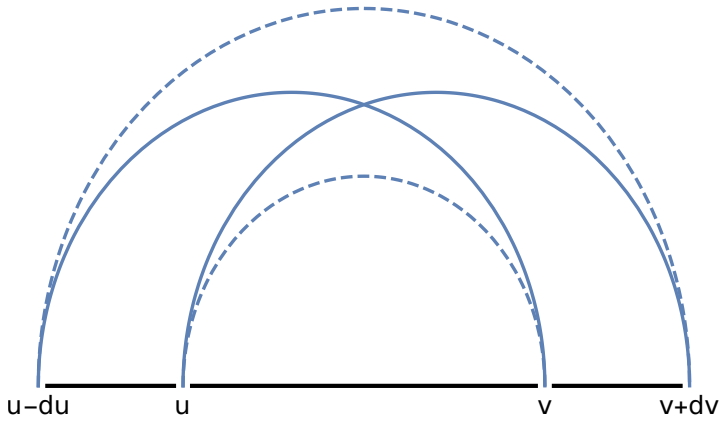

Figure 4.1: The curves are minimal geodesics bounding respective intervals, as called for by the Ryu-Takayanagi formula. This diagram illustrates the specific combination of geodesic lengths (refer eq. 4.1) which corresponds to the conditional mutual information, and the Crofton form on kinematic space. The same combination is constrained to be positive, in the strong-subadditivity inequality (refer eq. 4.2).

In our example of the Poincaré patch of AdS_2, with $S(u,v) \sim \frac{L}{2G}\log(v-u)$, we can calculate the Crofton form and the conditional mutual information to be

$$\omega_{K(\text{Poincaré patch})} = \frac{\partial^2 S(u,v)}{\partial u\,\partial v}\,du\,dv = \frac{L}{2G}\frac{du\,dv}{(u-v)^2}.$$

Note that the kinematic space metric, which corresponds to the Crofton form, has null directions and is therefore Lorentzian in signature.

In this example, exploiting translation invariance restrict $\omega_{K(AdS)} \equiv f(u-v)$ and then exploiting scale invariance helps restrict it to

$$\omega_{K(\text{Poincaré patch})} \sim \frac{du\, dv}{(u-v)^2}.$$

We therefore observe that the kinematic space corresponding to the Poincaré patch of AdS_2 turns out to be dS_2, and matches what we guessed based on its symmetries.

4.0.3 Multiscale Entanglement Renormalization Ansatz

Tensor networks are diagrams in the Penrose graphical tensor notation, used to illustrate the entanglement structure of many-body quantum wavefunctions. They can also be used as variational ansatzes to model such states, with each blob in the model representing parameters collected together as a tensor. When used as a variational ansatz, the tensor network provides a suitable description of a desired state only after a variational optimization. See ref. [192, 193] for a review of the topic, including motivations for tensor networks, and their applications.

The Multiscale Entanglement Renormalization Ansatz (MERA) is a particular class of tensor networks useful for modelling ground states of lattice models which are scale invariant under renormalization group flow (see ref. [186] for a review on the topic). Its network structure is depicted in figure 4.2. Each link or "bond" in the network could sum over a tensor index of any dimension; for simplicity, we take each link to have the same "bond dimension" χ. The fact that MERA could be considered a discrete real-space implementation of renormalization group flow makes it a particularly interesting object to study. The following key features make it very convenient for numerical calculations:

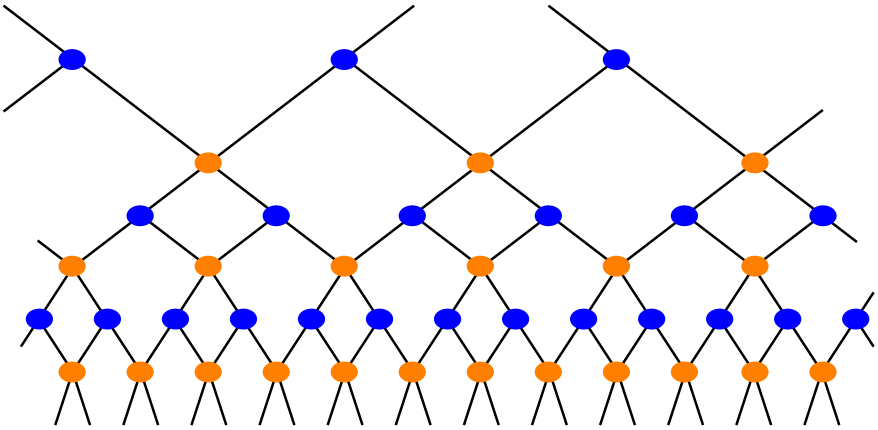

Figure 4.2: For a MERA network modelling the ground state of a conformal field theory, all isometries (blue) and all disentanglers (orange) are identical, motivated by translational and scale invariance.

- Heuristic identification of tensors motivated by translation and scaling symmetries of the quantum state drastically reduces the number of parameters to optimize variationally. As depicted in figure 4.2, a scale invariant MERA can be characterized by a single 'disentangler' tensor with $\mathrm{O}\left(\chi^4\right)$ and a single 'isometry' tensor with $\mathrm{O}\left(\chi^3\right)$ variational parameters respectively, since they are respectively constrained such that $u^\dagger u = \mathbf{1} = uu^\dagger$ and $w^\dagger w = \mathbf{1} \neq ww^\dagger$, as depicted in figure 4.3.

- The constraints on isometries and disentanglers enforce a causal structure in MERA computations, which makes possible an efficient calculation of local observables. In a contraction such as $\langle\psi|O(x)|\psi\rangle$, all tensors not in the inclusive causal cone of the region corresponding to x (see figure 4.4) cancel manifestly. Since the causal cone of the region has at most a constant number of tensors in each layer, such local observables can be efficiently computed.

Throughout the rest of this chapter, we will be referring to optimized MERA

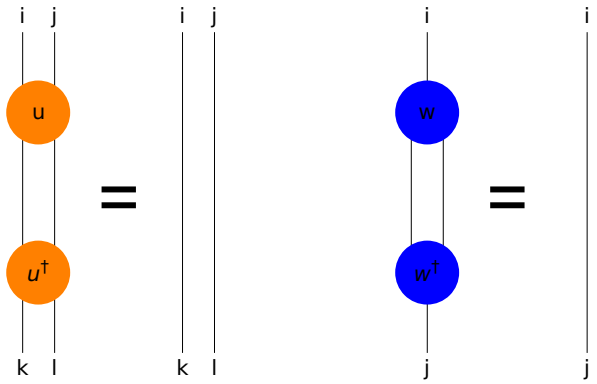

Figure 4.3: Graphical depiction of constraints on disentanglers u and isometries w.

networks. We also assume that all the gauge freedom in the network was used to exhibit it in a maximally symmetric form.

4.1 Minimal Updates

Consider a 1+1-dimensional CFT deformed by a localized defect. The defect traces a 0+1-dimensional world-line and introduces a preferred location in space. Thus, it breaks the global symmetry from $SO(2,2)$ down to $SO(2,1)$ or a subgroup thereof. We are interested in theories, where the full $SO(2,1)$ consistent with a defect is preserved. We shall refer to such theories as dCFTs, though it should be remembered that this class of theories includes interface and boundary CFTs. We emphasize that the symmetries of dCFTs do not include translations (broken by the defect), but do include scale transformations centered at points on the defect world-line.

The minimal updates proposal (MUP) [178] is a simple tensor network ansatz for the ground state wavefunction of a dCFT. As an input, it starts with an optimized MERA network representing the ground state of the undeformed (parent) CFT_2. The MUP asserts that a dCFT ground state can be captured by 'updating' in the input

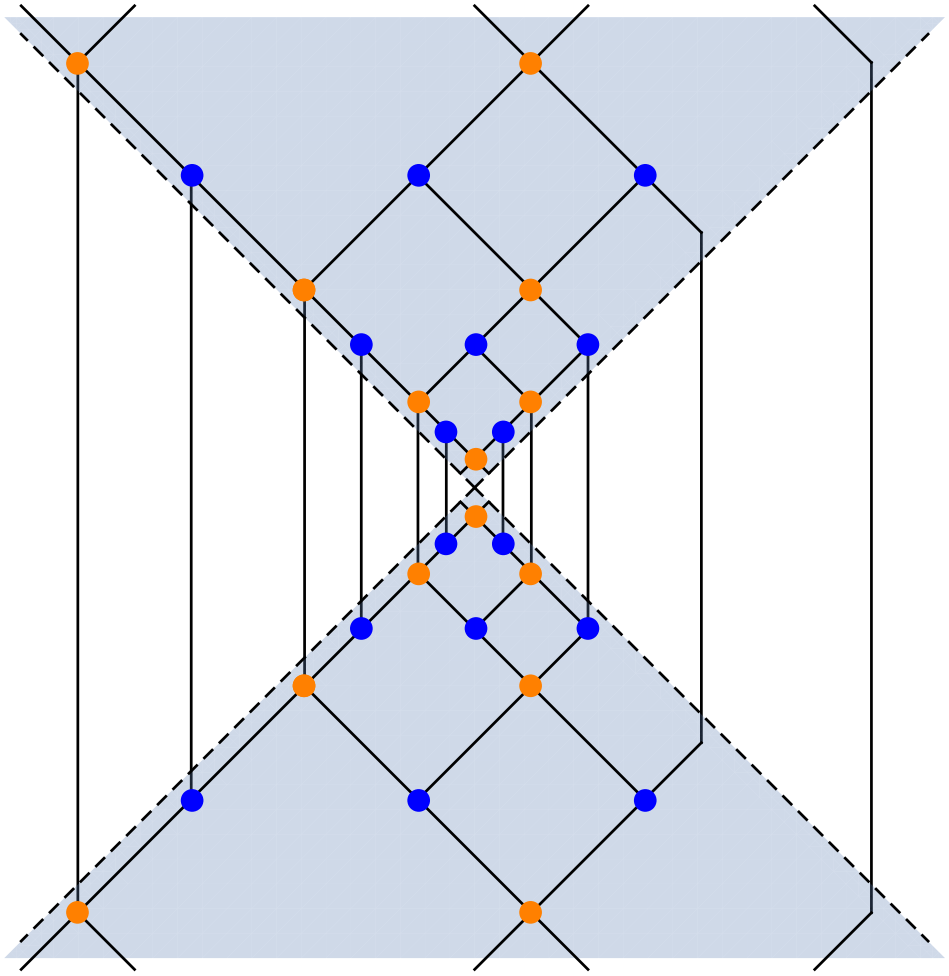

Figure 4.4: Simplification of observable computation in MERA, using constraints depicted in figure 4.3

MERA only those tensors, which live in the causal cone[4] of the defect location (see figure 4.5).

The MUP is a remarkably powerful ansatz. The computational simplifications owed to reusing the undeformed CFT ground state MERA are enormous. Empirically, the MUP achieves a remarkable accuracy on benchmark examples [178,185], including

[4]The 'causal structure' in MERA was introduced in ref. [156]; see ref. [165] for a discussion relevant to holographic duality.

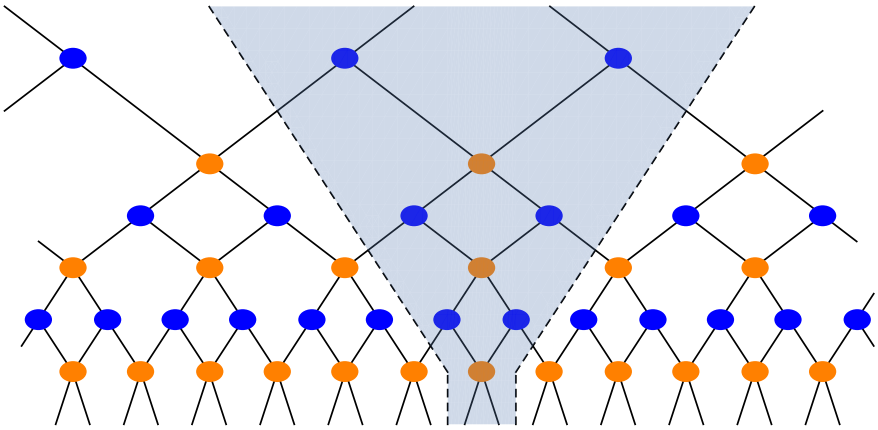

Figure 4.5: The inclusive 'causal cone' (shaded blue) of an operator insertion. The minimal updates prescription (MUP) specifies that on deforming a CFT by a defect, only the tensors in its inclusive causal cone need to be replaced in order to account for the defect.

the case of topological defects [194].

4.1.1 Rationales for Minimal Updates

Two rationales have been offered by its authors in support of minimal updates.

First, minimal updates guarantee that a local defect remains local after coarse-graining [178]. As explained in footnote 36 of that reference, initially allowing the update to extend away from the causal cone will, after optimization, lead to a generally location-dependent set of tensors: a defect not confined to a causal cone can 'spill out' under renormalization. The motivation behind MUP is to forestall this undesirable scenario. This rationale, however, is not a proof of validity. The symmetry of the problem does not guarantee that tensors in the description of a dCFT ground state are location-independent (see section 4.2 below.)

Second, there is an algorithmic procedure which takes a discretized (Trotter-Suzuki) version of the Euclidean path integral and transforms it into a MERA repre-

sentation of the ground state [195]. In effect, Tensor Network Renormalization (TNR) is a derivation of MERA. Applied to Euclidean path integrals of dCFTs, TNR can return a MERA network with a structure predicted by MUP [196]. This seems to provide a derivation of minimal updates, but here too there is a caveat. A key step in TNR is a local substitution of tensors in the discretized path integral, which is justified by bounding the resulting error (cost function) to a desired tolerance. When the cost function takes into account only the local environment of the tensor to be replaced, the TNR algorithm yields the minimally updated MERA. However, as discussed in section VIII (B) of ref. [194], the TNR algorithm with a global cost function may not produce a MERA with the MUP-dictated structure. Since the conditions under which it suffices to work with a local environment are not known, the status of this second rationale for MUP is also unclear.

In summary, refs. [178] and [196] give two independent rationales for the validity of the minimal updates proposal, neither of which is foolproof. Here we offer a third argument, which relies on symmetry and known properties of dCFTs:

4.1.2 Minimal Updates and the Boundary Operator Expansion

A key new ingredient in a dCFT is the appearance of the Boundary Operator Expansion (BOE) [197, 198]:

$$\mathcal{O}_\eta(x) = \sum_i \frac{B_{\mathcal{O}_\eta}^{\hat{\mathcal{O}}_{\hat{\eta}_i}}}{(2y)^{\eta-\hat{\eta}_i}} \hat{O}_{\hat{\eta}_i}(\mathbf{x}) \tag{4.3}$$

Here we set up coordinates $x = (y, \mathbf{x})$ where y is the direction perpendicular to the defect and $\mathbf{x}$ are the directions along the defect world-volume. Hats mark operators living on the codimension-1 world-volume of the defect. In the formula above we also

assumed that $\hat{O}_{\hat{\eta}_i}$ are scaling operators, i.e. they have well-defined scaling dimensions $\hat{\eta}_i$ under dilations centered at the defect location. The BOE allows us to decompose the action of any local operator according to irreducible representations of the residual $SO(1,2)$ symmetry.

In an ordinary CFT all correlation functions can in principle be reduced to kinematic invariants multiplied by products of OPE coefficients, which are the only dynamical data in the theory. In a dCFT, there is an analogous statement: the complete set of dynamical data consists of the BOE coefficients $B^{\hat{\mathcal{O}}_{\hat{\eta}_i}}_{\mathcal{O}_\eta}$ together with the familiar OPE coefficients used for fusing operators away from the defect. For example, one-point functions of local operators in a dCFT are generically non-vanishing and can be read off from fusing the local operators with the defect using the BOE:

$$\langle \mathcal{O}_\eta(x) \rangle = \frac{B^{\hat{1}}_{\mathcal{O}_\eta}}{(2y)^\eta} \tag{4.4}$$

Similarly, a correlation function of two local away-from-defect operators $\mathcal{O}_{\eta_1}$ and $\mathcal{O}_{\eta_2}$ can be obtained by first fusing them using the OPE into $\mathcal{O}_\eta$ and then applying eq. (4.4) or, in a different channel, by sequentially fusing $\mathcal{O}_{\eta_1}$ and $\mathcal{O}_{\eta_2}$ with the defect via a double application of the BOE.

To verify the validity of the minimal updates proposal, we only need to confirm that the ansatz is powerful enough to correctly encode the away-from-defect OPE and the BOE coefficients. It is well known that the optimized tensors of the ordinary MERA essentially compute the OPE coefficients of a CFT. This is manifest in the way in which OPE coefficients are extracted from MERA; see e.g. ref. [199]. By reusing the undeformed CFT ground state MERA, the minimal updates proposal effectively borrows the undeformed theory's OPE coefficients for fusing away-from-defect local operators. Indeed, a ground state ansatz that departs from the minimally updated MERA would contaminate the fusion rules for operators applied away from

the defect.

The above logic implies that the role of the updated region is to encode the remaining dynamical data—the BOE coefficients. Is the ansatz powerful enough to do so? As a computational problem, finding the correct update has the same structure (the same set of inputs and outputs) as the problem of finding the OPE coefficients in the familiar applications of MERA to ordinary CFTs. In both cases, we are looking for tensors that represent a super-operator, which fuses two given sets of operators into one. This argument reduces the question of the validity of the MUP for describing dCFT ground states to the long-settled question of whether the ordinary MERA captures ground states of ordinary CFTs.

This justification for the MUP was not spelled out in ref. [178] or subsequent papers, though similar arguments appeared in ref. [230]. We believe it is important to emphasize the relation between minimal updates and the dCFT technology, especially with a view to the following generalization.

4.2 Rayed MERA

Thus far we have considered dCFTs—theories obtained from ordinary CFTs by introducing codimension-1 defects. In general, however, the class of two-dimensional theories with $SO(2,1)$ invariance is much larger. One way to obtain such a theory is by a deformation and (if the deformation is not exactly marginal) an RG flow to a new fixed point. To preserve the symmetry, the sources entering the deformation should have a power-law dependence with y, the distance from the world-line fixed by the $SO(2,1)$ symmetry. Still more generally, we can consider a more abstract CFT-like theory in which 'OPE coefficients' for fusing $\mathcal{O}_i(x)$ and $\mathcal{O}_j(x')$ have an explicit

dependence on

$$\xi = \frac{(x - x')^2}{4yy'}\,, \tag{4.5}$$

which is the $SO(2,1)$ invariant built from x and x' discussed e.g. in ref. [197].

Representing the ground state of a generic, two-dimensional, $SO(2,1)$-invariant theory is outside the scope of the minimal updates proposal. For an arbitrary such theory, there may not exist a CFT whose ground state MERA could be appropriately minimally updated. This is most easily recognized when we consider 'OPE coefficients' that depend on ξ from eq. (4.5). We observed previously that in the minimally updated MERA, the region that is directly imported from the parent MERA is responsible for correctly merging away-from-defect operators according to the fusion rules of the parent theory. A theory with ξ-dependent 'OPE coefficients' does not emulate the fusion rules of any parent theory.

Despite the huge freedom in constructing two-dimensional $SO(2,1)$-invariant theories, it is possible to write down a simple MERA-like ansatz, which ought to capture the ground states of such theories? To do so, note that the tensor network is supposed to represent the wavefunction of the theory at an equal time slice. The only generator of $SO(2,1)$ that acts within a time slice builds dilations about the origin—where the 'defect' (the world-line fixed by $SO(2,1)$) and the time slice intersect. The action of the conformal group on the MERA network was studied in ref. [166] (see also ref. [200]). It was found that the orbits of dilations about the origin are tensors, which live on rays emanating from the origin. Thus, the invariance under $SO(2,1)$ dictates that all tensors inhabiting the same ray must be identical, though tensors living on different rays may be distinct. Such an ansatz, which we call **rayed MERA**, is displayed in figure 4.6.

Several remarks are in order. First, the minimally updated MERA is a special

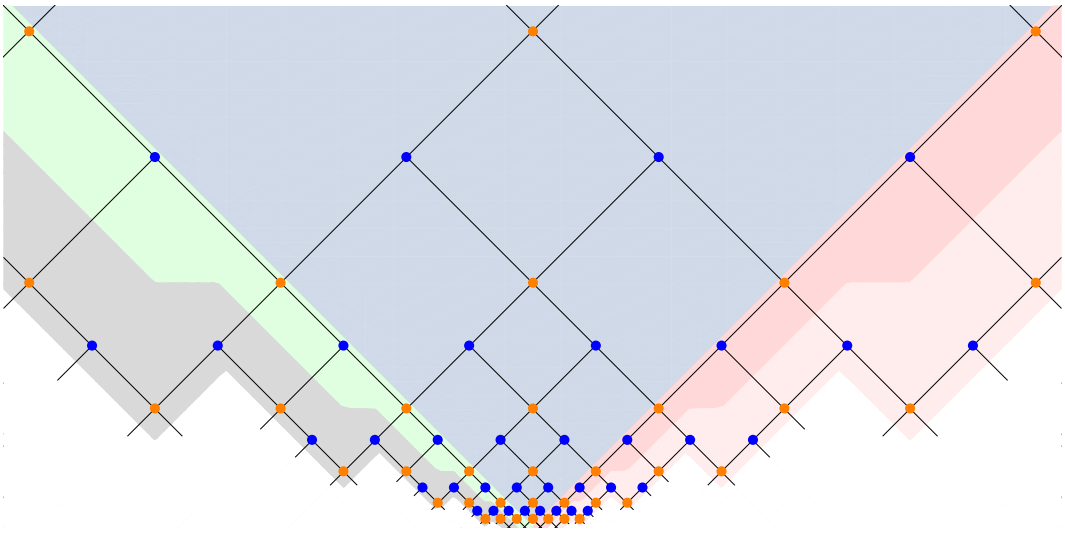

Figure 4.6: Rayed MERA: Tensors on each 'ray' (color coded) are the same because they are related by a scaling symmetry about the origin (defect location). Tensors inhabiting different rays are in general distinct.

case of the rayed MERA in which only the vertical ray is distinct from the others. Second, distinct rays are labeled by different values of:

$$\xi = \frac{(x-x')^2}{4yy'} \quad \xrightarrow[\text{(equal time)}]{\mathbf{x}=\mathbf{x}'} \quad \frac{(y-y')^2}{4yy'}\,. \tag{4.6}$$

Here y and y' denote a pair of locations such that if two local operators are inserted there, their causal cones will merge on the ray labeled by ξ. If we think of local groups of tensors as encoding OPE coefficients, making the tensors explicitly dependent on ξ amounts to choosing ξ-dependent 'OPE coefficients.' In the minimally updated MERA, the only ξ-dependence distinguishes the parent OPE coefficients from the BOE coefficients, which are encoded on the vertical ray.

4.3 Holographic Interpretations

We will now look at two holographic realizations of interface CFTs and discuss how, if at all, they relate to either the minimally updated MERA of ref. [178] or the rayed MERA of section 4.2. To set the context for our discussion, let us briefly recap how prior proposals related the ordinary MERA to pure anti-de Sitter space.

MERA and holography without defects Ref. [157] observed a resemblance between the MERA network and a static slice of AdS_3, i.e. the hyperbolic disk. Both have a self-similar structure near the cut-off surface and both contain closely related notions of a minimal cut. Geodesics in AdS_3, which by the Ryu-Takayanagi proposal compute entanglement entropies of CFT_2 regions, resemble minimal cuts through the MERA network. This correspondence is consistent insofar as every bond in a minimal cut through MERA contributes an equal amount to the entanglement entropy of the subtended CFT region. Based on the conclusions of ref. [166], we recognize this fact (first observed in ref. [155]) as a consequence of the $SO(2,2)$ symmetry of the CFT.

The kinematic proposal of refs. [164, 165] instead views individual tensors in MERA as discrete counterparts of geodesics. This does not run into obvious contradictions with ref. [157] because every minimal cut in MERA selects a unique tensor, which lives in its top corner. In the kinematic proposal, a key to understanding geodesic lengths and entanglement entropies is the Crofton formula, which schematically reads [164]:

$$\text{length of a curve} = \int_{\text{intersecting}} \mathcal{D}\,(\text{geodesics}). \tag{4.7}$$

Here $\mathcal{D}$ (geodesics) is the unique measure over the set of geodesics in $\mathbb{H}_2$ invariant under its isometries. The correspondence between MERA tensors and geodesics ad-

vocated in ref. [165] translates eq. (4.7) into simply counting tensors in certain regions of the MERA network.

4.3.1 Thin Wall Models: A Naïve Realization of Minimal Updates

Note that under both holographic interpretations, the directly imported (i.e. not updated) regions of the MUP MERA account for two halves of (the spatial slice of) pure anti-de Sitter space. This is most obvious in the kinematic interpretation: the unaltered regions consist of geodesics with both endpoints on the same side of the defect and both sets (left and right of defect) of such geodesics span one half of the hyperbolic disk. In the original proposal of ref. [157], the minimally updated region should be viewed as a discrete counterpart of a radial geodesic, with one half of $\mathbb{H}_2$ on each side of it. This is because MERA does not accommodate a notion of locality narrower than the width of one causal cone [199]. Whichever proposal we adopt, the regions that remain unaltered by the minimal updates should be viewed as two halves of the hyperbolic disk, each ending on a geodesic diameter.

From this observation, one could venture the following, **naïve holographic interpretation** of the minimal updates proposal: that the holographic dual of a dCFT should contain two undeformed halves of pure anti-de Sitter space separated by some 'wall.' Whatever the wall is, on either side of it should be (at least) one half of pure anti-de Sitter space.

We shall see later that this holographic reading of the minimal updates proposal is too naïve because it is too stringent. But before that, let us inspect a class of models that realize this naïvely stringent interpretation of minimal updates:

Thin wall models Consider a simple toy model for the holographic dual of a dCFT, which consists of two AdS_3 patches glued together with a tensionful brane. Such models were discussed for example in refs. [201–204] (for early geometric analyses see refs. [205, 206]), building up on an embedding in string theory [179, 180]. As we clarify below, the holographic duals of boundary CFTs discussed in refs. [182–184] also fall into this class.

The setup is illustrated in figure 4.7. The two AdS patches can have different curvatures, which would correspond to coupling along an interface two CFTs with central charges c_L and c_R respectively. (The special case $c_L = c_R \equiv c$ are actual defect CFTs, as opposed to the more general variety of interface CFTs.) The famous Brown-Henneaux formula [207] relates the central charges to the radii of curvature:

$$\frac{L}{G} = \frac{2}{3}c_L \qquad \text{and} \qquad \frac{R}{G} = \frac{2}{3}c_R. \tag{4.8}$$

Here G is the bulk Newton's constant and L, R are the AdS radii on the two sides.

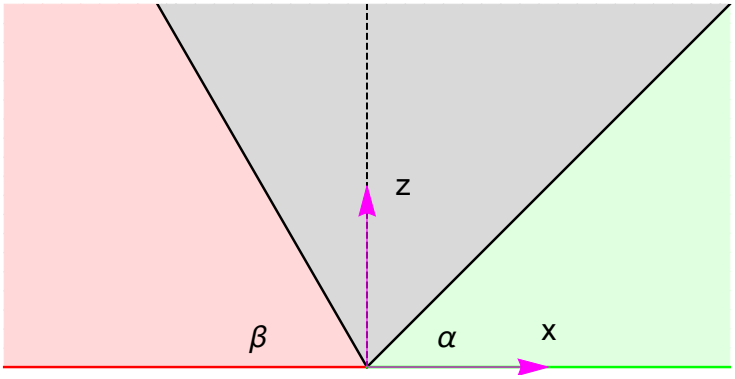

Figure 4.7: A thin wall geometry consists of two wedges of pure AdS_3 (pink and green regions) glued along a tensionful wall. The wall occupies a 'straight line' in the Poincaré coordinates, which delimits each AdS_3 chunk. The two straight lines are identified.

We will adopt the familiar Poincaré patch coordinates (x, z) on both sides of the

brane:

$$ds^2 = L^2 \frac{-dt^2 + dx^2 + dz^2}{z^2} \qquad \text{and} \qquad ds^2 = R^2 \frac{-dt^2 + dx^2 + dz^2}{z^2} \tag{4.9}$$

The wall occupies a surface of constant extrinsic curvature, which in this coordinate system turns out to be a 'straight line' in the z-x plane. Each patch of AdS_3 on one side of the wall is characterized by the slope of that line, which we express in terms of α and β:

$$z = -x \tan\beta \ \ \text{(left)} \qquad \text{and} \qquad z = x \tan\alpha \ \ \text{(right)} \tag{4.10}$$

Figure 4.7 depicts one example geometry, in which α and β are both less than $\pi/2$. Note that $\alpha = \pi/2$ denotes one half of the hyperbolic disk delimited by a radial geodesic. Thus, the naïve holographic interpretation of minimal updates predicts that $\alpha, \beta \geq \pi/2$.

We now verify that the thin wall models conform to this prediction.

In the thin wall geometry, Einstein's equations reduce to the Israel junction conditions [229], which we re-derive in Appendix A.1. For a brane of tension λ, these take the form:

$$\frac{L}{\sin\beta} = \frac{R}{\sin\alpha} = -\frac{\cot\alpha + \cot\beta}{8\pi G\lambda} \,. \tag{4.11}$$

These three quantities are equal to the radius of intrinsic curvature on the brane. Observe that eqs. (4.11) accommodate the duals of boundary CFTs discussed in refs. [182–184] simply by setting $\beta = \pi/2$. This introduces a fictitious left chunk of AdS_3 with curvature $L = R/\sin\alpha$ which decouples, because it exerts no force on the bulk wall.

Although eqs. (4.11) have formal solutions with arbitrary α and β, in fact only $\alpha, \beta \geq \pi/2$ are physical. When $\alpha, \beta < \pi/2$, the tension λ is forced to be negative,

which violates the weak energy condition in the bulk.[5] Such a situation gives rise to rather exotic features associated with strong subadditivity, which we detail in Appendix A.2.

The remaining case, $\alpha \geq \pi/2 > \beta$, is also unphysical. As we show in Appendix A.1, in this regime the wall is necessarily unstable so it cannot be the dual of the ground state of a dCFT.

Studying geodesics in the thin wall space-time built by a wall with positive tension turns out to involve an interesting application of Snell's law. Because we have not found a solution of this problem anywhere in the literature, in Appendix A.2 we explain how to find such geodesics and compute the kinematic space of the thin wall geometry.

Summary The thin wall geometry is consistent with the naïve holographic interpretation of the minimally updated MERA. This is true regardless of whether we adopt the direct [157] or the kinematic [165] proposal for relating MERA to holographic geometries.

However, the direct proposal is arguably subject to some awkward caveats. This is because $\alpha, \beta > \pi/2$ means that the thin wall geometry is strictly larger than it would have been in the absence of a defect. Thus, the causal cone of the defect must be simultaneously interpretable as the radial geodesic (in the dual of the undeformed CFT) and as the extra thickness of space-time grown by the thin wall (quantified by $\alpha + \beta - \pi$.) This caveat does not arise in the kinematic proposal where, with or without the wall, we are always dealing with the same set of geodesics. We will not dwell on this issue further because more general models will anyway force us to revise

[5] Ref. [204] contains a thorough discussion of energy conditions in the context of holographic dCFTs.

our assumptions.

4.3.2 Thick Walls: Not All Bonds Are Created Equal

The exercise of studying thin wall models is useful because it immediately illustrates why the 'naïve holographic interpretation' of the minimally updated MERA is naïve. As soon as our wall is no longer thin, it will involve non-trivial profiles of various bulk fields whose tails extend all the way to the asymptotic boundary. Indeed, the non-vanishing one-point functions (4.4) of holographic dCFTs are read off precisely from such tails of normalizable modes of bulk fields. Looking for two greater-than-half chunks of pure AdS_3 on both sides of the wall can only work in a thin wall model.

There is another reason why the naïve interpretation is too naïve. When we discussed the direct [157] and the kinematic [165] readings of MERA, the full $SO(2,2)$ symmetry of the theory appeared to be a key ingredient. In the direct proposal, the connection between minimal cuts in MERA and geodesics in AdS_3 was only sensible because every MERA bond contributed an equal amount to the entropy count [155]. This feature relies on the global $SO(2,2)$ symmetry. To see this, recall that changing the UV cut in MERA corresponds to applying a conformal transformation [166]. Any bond in MERA can become a part of the UV cut under the action of $SO(2,2)$ and therefore all bonds are related to one another by this symmetry. In the kinematic proposal, on the other hand, the $SO(2,2)$ entered via the choice of measure $\mathcal{D}$ (geodesics), which translated into uniformly counting different MERA tensors.

In the case at hand, the symmetry is broken to $SO(2,1)$. On the spatial slice modeled by the tensor network, the only symmetry we have are dilations about the origin. In order to relate thick wall models to MUP, we must assign different weights to different tensors and bonds in the minimally updated MERA.

Assigning relative weights to bonds and tensors Ref. [165] explained how to weigh different regions of MERA in the kinematic interpretation. To explain this prescription, we need a few basic facts.

In the present context, the kinematic space is the space of intervals on a spatial slice of a CFT_2. When a holographic dual is available, it is also the space of bulk geodesics. The kinematic space has a Lorentzian metric of the form:

$$ds^2_{\text{K.S.}} = \frac{\partial^2 S_{\text{ent}}(u,v)}{\partial u \partial v}\, du dv\,, \tag{4.12}$$

where u and v are the two endpoints of a CFT interval / bulk geodesic and S_{ent} is the entanglement entropy of the interval / length of the geodesic. This metric turns out to be de Sitter space in the case of a locally AdS geometry, and has many attractive properties which were discussed in refs. [164, 165] and elsewhere [208–211]. For example, the volume form derived from this metric defines a measure on the space of bulk geodesics $\mathcal{D}$ (geodesics) such that eq. (4.7) holds.

The claim of ref. [165] is that we can think of MERA as a discrete version of kinematic space. To do so, consider two pairs of nearby points, $(u, u-\Delta u)$ and $(v, v+\Delta v)$, on the UV cut of MERA. We can impose on MERA a discretized version of metric (4.12):

$$ds^2_{\text{MERA}} = S_{\text{ent}}(u-\Delta u, v) + S_{\text{ent}}(u, v+\Delta v) - S(u-\Delta u, v+\Delta v) - S(u,v)\,. \tag{4.13}$$

In this 'metric', the light-like directions u and v agree with the causal structure of MERA, which we mentioned in section 4.1. The quantity (4.13) coincides with a discretized 'volume form' on the tensors of MERA, which can be compared with $\mathcal{D}$ (geodesics).

In the ground state of an $SO(2,2)$-invariant theory, eq. (4.13) defines a discrete version of two-dimensional de Sitter space.[6] But in a theory with only $SO(2,1)$

[6] For other observations relating MERA to de Sitter space, see refs. [212, 213].

invariance, the 'volumes' assigned to different regions of MERA will differ. The only fact guaranteed by the symmetry is that identical regions living on the same ray (as discussed in section 4.2) carry equal volumes.

A case study in thick walls: the AdS$_3$-Janus solution One holographic pair which illustrates this non-uniformity is the Janus deformation of AdS$_3$ and its dual interface CFT. Following earlier developments in AdS$_5$ [214], refs. [181,215–219] studied a scalar field ϕ (the 'dilaton') coupled to Einstein gravity with a negative cosmological constant in three dimensions and found the following solution:

$$ds^2 = L^2 \left(du^2 + \rho(u)^2 \, ds^2_{AdS_2}\right) \tag{4.14}$$

$$ds^2_{AdS_2} = -\cosh^2 r dt^2 + dr^2 \tag{4.15}$$

$$\rho(u)^2 = \frac{1}{2}(1 + \sqrt{1-2\gamma^2}\cosh 2u) \tag{4.16}$$

$$\phi(u) = \phi_0 + \frac{1}{\sqrt{2}} \log\left(\frac{1+\sqrt{1-2\gamma^2}+\sqrt{2}\gamma\tanh u}{1+\sqrt{1-2\gamma^2}-\sqrt{2}\gamma\tanh u}\right) \tag{4.17}$$

They also explained how this solution is holographically dual to the ground state of a marginal deformation of the D1-D5 CFT whose strength is proportional to γ. The deformation has a different sign on the two halves of the boundary, so the resulting theory is an interface CFT. In the bulk, the AdS$_3$-Janus solution contains a thick wall.

We do not have an optimized tensor network which prepares the ground state of this theory, so we cannot make quantitative comparisons with MERA. But we can compute its kinematic space (eq. 4.12) and observe qualitative features. We carried out this computation for small γ in Appendix A.3. Up to an overall factor of $L/2G$, the result, to first non-trivial order in γ, reads:

$$ds^2_{\text{K.S.-Janus}} = \frac{du\,dv}{(u-v)^2}\left[1 - \frac{\gamma^2}{2}\left(\eta^2 + 3 - \frac{1}{2}\left(\eta^3 + 3\eta^{-1}\right)\log\left|\frac{1+\eta}{1-\eta}\right|\right)\right] \tag{4.18}$$

Here $\eta = (v-u)/(v+u)$ is a kinematic $SO(2,1)$ invariant, related to ξ from eq. (4.5) via:

$$\eta = (\xi^{-1} + 1)^{-1} \,. \tag{4.19}$$

The inside of the causal cone of the interface has $\eta > 1$ while the regions in MERA that are imported from the parent without updates have $\eta < 1$. Indeed, the effect of the interface spills out beyond the causal cone of the interface, and increases the kinematic volume there. It is UV-finite and in fact vanishes in the UV limit $\eta \to 0$, where the effect of the interface is the smallest.

Within the causal cone, on the other hand, the interface causes the overall kinematic volume to decrease. This is to be expected because according to eq. (4.7) the volume of this region computes the entanglement entropy of the two sides of the interface.

Summary: The bulk duals of holographic dCFTs generically involve thick walls. In relating such theories to tensor networks, we cannot count all tensors or bonds with equal weight. Instead, we must account for different weights that occur at different values of the $SO(2,1)$ invariant ξ (see eq. 4.5). In a minimally updated MERA, even though all tensors outside the causal cone are identical, their weights differ depending on the location relative to the defect.

4.3.3 Non-normalizable Modes: From the Minimally Updated MERA to Rayed MERA

The above conclusion poses one residual question. On the one hand, the MUP mandates that some tensors do not register the presence of a defect; on the other hand, those tensors count with different weights when we calculate entropies. What then

distinguishes states constructible using the minimally updated MERA versus the rayed MERA? We would like to answer this question in a way that makes contact with the AdS/CFT correspondence.

Recall that the minimally updated MERA is designed for theories constructed by coupling two $SO(2,2)$ invariant parent theories along a common interface. The rayed MERA is for a generic $SO(2,1)$-invariant theory, which could be constructed in multiple ways. One such way is to deform a parent theory by an appropriately selected source, which is either $SO(2,1)$-invariant or designed to recover the $SO(2,1)$ after an RG flow. In holography, deforming theories by the introduction of sources is effected by turning on non-normalizable modes in the bulk [220]. Thus, a ground state of a holographic theory whose bulk dual involves a thick wall can be prepared by either one of the two types of networks—the minimally updated MERA or the rayed MERA—depending on whether the thick wall contains condensates of non-normalizable modes away from the 'interface.' Here by 'interface' we mean the fixed world-line of the residual $SO(2,1)$ symmetry.

As an example, the holographic dual of the AdS_3-Janus solution is a marginal deformation of the D1-D5 CFT [181]:

$$S = S_{\text{D1D5}} + \tilde{\gamma} \int_{x>0} dx\, dt\, \mathcal{O}_\phi(x,t) - \tilde{\gamma} \int_{x<0} dx\, dt\, \mathcal{O}_\phi(x,t) \tag{4.20}$$

Here $\tilde{\gamma}$ is a deformation parameter, which agrees with the γ from eqs. (4.16) and (4.17) to leading order, $\tilde{\gamma} = \gamma + O(\gamma^2)$. The bulk solution involves a non-normalizable mode for the dilaton, which asymptotes to different constant values on the boundary

$$\phi \to \phi_\pm = \phi_0 \pm \frac{1}{\sqrt{2}} \tanh^{-1} \sqrt{2}\gamma \tag{4.21}$$

and accounts for the deformation (4.20).

Eq. (4.20) is a marginal deformation of the parent CFT with a piece-wise constant source that jumps at the interface. If, in principle, we had at our disposal MERA representations of the ground states of the theories

$$S = S_{\text{ D1D5}} \pm \tilde{\gamma} \int_{\text{all } x} dx\, dt\, \mathcal{O}_{\phi}(x,t)\,, \tag{4.22}$$

we could use them as input in the minimal updates prescription. Thus, the ground state of the theory dual to the AdS_3-Janus solution belongs to the class of states, which can in principle be represented in the form of a minimally updated MERA. Of course, the tensors comprising that network would be different from those which prepare the ground state of the undeformed theory.

However, if we turn on more general deformations while preserving $SO(2,1)$, the resulting ground states can only be prepared using the rayed MERA. For example, we could deform a holographic CFT with irrelevant operators coupled to sources with a power-law dependence on the distance from a select line. If the interior of the resulting bulk geometry were then compared to a MERA-type tensor network, it would have to be a rayed MERA.

Summary: The distinction between the minimally updated MERA and the rayed MERA is whether we simply couple two parent CFTs along an interface or do something more generic, such as to change the fusion rules. A theory in the latter category is generally outside the scope of the minimal updates prescription, but if it preserves $SO(2,1)$ symmetry, it can in principle be captured by a rayed MERA.

4.4 Discussion

There is now a considerable literature which seeks ways to relate spacetimes that arise in holographic duality to tensor networks. The paper on which this chapter is based summarizes the next step in this endeavor: studying space-times which are neither pure anti-de Sitter nor its quotients nor Virasoro descendants. For this initial study we chose to consider holographic defect, interface and boundary CFTs (dCFTs) and tensor networks in the class of the Multi-scale Entanglement Renormalization Ansatz (MERA).

We concentrated on MERA for 1+1-dimensional CFTs because this class of networks is best understood. In particular, in MERA we know (a) how to realize conformal transformations (by changing the UV cut [166]), (b) how the spectrum of conformal dimensions and OPE coefficients are encoded (for details, see ref. [199]), and (c) how to represent ground states of dCFTs (the minimal updates proposal [178]). Concerning the class of theories, we focused on dCFTs because they obey a residual $SO(2,1)$ global symmetry, which has a clarifying power. It organizes data in both MERA (on rays emanating from the origin) and in the holographic geometry (which is foliated by AdS_2 slices.)

Some of our conclusions concern specifically the MERA class of tensor networks. We clarified and complemented arguments supporting the validity of the minimal updates proposal (section 4.1) and proposed an extension for generic, $SO(2,1)$-invariant theories (rayed MERA, section 4.2). Our other conclusions should hold more generically. In particular, we expect that in every meaningful instance of a holographic bulk geometry-tensor network correspondence, the following rule should hold:

- Changing tensors in the ground state network represents turning on non-normalizable

modes in the bulk.

In the case of MERA, because of its causal structure, the effect of locally turning on a non-normalizable mode is contained in the causal cone of the deformation. We propose this as the holographic interpretation of the theory of minimal updates [178]. But in other types of networks such as those in refs. [221–225], the effect of a deformation should also be cleanly identifiable and likely localized in a subregion of the network.

At the same time, we should remember that local properties of a tensor network state in general depend non-locally on the tensors. One example considered in this chapter (see section 4.3.2) is the set of entanglement entropies, which underlie both the direct [157] and the kinematic [165] holographic interpretation of MERA. We can think of such local but non-locally determined properties of tensor network states as akin to the normalizable bulk modes. In AdS/CFT, these encode responses to boundary conditions set elsewhere. Other familiar examples of such quantities are CFT one-point functions, which in MERA depend on the entire causal future of the given point.

Next steps It would be interesting to realize some of these ideas in other types of tensor networks, which were specifically designed for the AdS/CFT correspondence [221–225], and also consider the Kondo problem as an example [226]. Many questions await answers: How do these networks encode OPE coefficients of the CFT? Can we see how deforming the CFT changes the ground state tensors and thus observe the effect of a non-normalizable mode? How to represent ground states of defect CFTs? More specifically, how to deform those networks to construct an analogue of a thin wall geometry? This last problem is further pertinent for understanding how

those classes of tensor networks can accommodate the backreaction of bulk matter fields.

Departing from tensor networks, ref. [150] (on which this chapter is based) is the first study of the kinematic space of dCFTs. For ordinary CFTs, studying fields *local in kinematic space* led to enlarging the holographic dictionary by the addition of OPE blocks, which at leading order in $1/N$ are dual to bulk fields integrated along geodesics [208,209]. It would be interesting to generalize these findings to holographic dCFTs, perhaps starting with thin wall bulk duals. Interesting work in this direction followed in ref. [227].

Appendix

A.1 Israel Junction Conditions and Wall Stability

We consider three-dimensional geometries, which preserve $SO(1,2)$ symmetry:

$$ds^2 = du^2 + \rho(u)^2(-\cosh^2 r dt^2 + dr^2) \tag{A.1}$$

For a dual of a general holographic dCFT, we should also include other fields and their backreactions; one such example is discussed in section 4.3.2 and Appendix A.3. Here we assume that the geometry contains a thin wall of tension λ. To have a locally AdS_3 geometry to the left of the wall, we must have

$$\rho(u) = L\cosh(u/L), \tag{A.2}$$

where L is the left AdS_3 curvature radius. To the right of the wall, we will have a similar expression with $L \to R$, the curvature radius on the right. On the static slice $t = 0$, the change of coordinates from (A.1) to (4.9) is:

$$z = e^r \operatorname{sech} u/L \qquad \text{and} \qquad x = -e^r \tanh u/L\,. \tag{A.3}$$

Away from a spatial slice the formulas are more involved, but we do not need them in this paper.

In eq. (A.2), the asymptotic boundary of space-time is approached as $u \to -\infty$ while the wall sits at some specific value u_*. The $u = 0$ slice of metric (A.1) is a minimal surface in AdS_3, so depending on the sign of u the constant-u slices are contracting (for $u < 0$) or expanding (for $u > 0$) in the direction of increasing u, that is toward the wall. This distinction will be important for our considerations.

To find a static configuration of the AdS_3 chunks and the wall, we consider the Einstein-Hilbert action with a Gibbons-Hawking-York (GHY) term and an explicit wall contribution:

$$S = \frac{1}{16\pi G}\int_{\text{left}} d^3x\sqrt{-g}(\mathbf{R}-2\Lambda)+\frac{1}{8\pi G}\int_{\text{wall}} d^2y\sqrt{-h}K_L+(L\to R)-\lambda\int_{\text{wall}} d^2y\sqrt{-h} \tag{A.4}$$

Additional GHY terms arise at the asymptotic boundary of space-time, but these will play no role in our analysis. The Ricci scalar in metric (A.1) takes the form:

$$\mathbf{R} = -2\,\frac{1+\rho'^2+2\rho\rho''}{L^2\rho^2} \tag{A.5}$$

We can confirm the correctness of this expression by substituting (A.2), which gives $\mathbf{R} = -6/L^2$. Plugging eq. (A.5) and $\Lambda = -L^{-2}$ into (A.4), the action takes the form:

$$S \propto -\frac{L}{8\pi G}\int^{u_*} du\left(1+\rho'^2+2\rho\rho''-\rho^2\right)+\frac{L^2\rho(u_*)^2K_L}{8\pi G}+(L\to R)-L^2\rho(u_*)^2\lambda \tag{A.6}$$

Here we have dropped an overall infinite factor, which stands for the volume of AdS_2 with unit curvature.

Expression (A.6) contains two terms, which can be combined and simplified. To get a standard variational problem, we need to eliminate ρ'' via integration by parts. This introduces a boundary term, which the GHY term is designed to cancel:

$$-L\int^{u_*} du\,2\rho\rho''+L^2\rho(u_*)^2K_L = -L\int^{u_*} du\,2\rho\rho''+L\frac{d}{du}\rho^2\Big|_{u_*} = L\int^{u_*} du\,2\rho'^2 \tag{A.7}$$

After this substitution, action (A.6) becomes:

$$S = \frac{L}{8\pi G}\int^{u_*} du\left(\rho'^2-1+\rho^2\right)+(L\to R)-L^2\rho(u_*)^2\lambda \tag{A.8}$$

We may now plug in the known solution (A.2) for $\rho(u)$ and its right counterpart to obtain:

$$S = \frac{L}{4\pi G}\int^{u_*} du\,\sinh^2 u+\frac{R}{4\pi G}\int^{v_*} dv\,\sinh^2 v-\lambda\,L^2\cosh^2 u_*. \tag{A.9}$$

For continuity of the metric, the intrinsic geometry of the wall must be the same in both the u and v metrics. This leads to the first Israel junction condition [229], which is the first equality in eq. (4.11):

$$L\cosh u_* = R\cosh v_*. \tag{A.10}$$

Note that we have two distinct branches of v_*, which correspond to having a 'smaller-than-half' or 'bigger-than-half' chunks of AdS_3 to the right of the wall:

$$\sinh v_* = \pm\sqrt{(L/R)^2\cosh^2 u_* - 1} \tag{A.11}$$

To the left of the wall, the analogous distinction is controlled by the sign of u_*.

It is now trivial to find the equilibrium configuration of the AdS_3 patches and the wall. Setting $dS/du_* = 0$ gives:

$$\frac{L}{4\pi G}\sinh^2 u_* + \frac{R}{4\pi G}\sinh^2 v_* \cdot \frac{dv_*}{du_*} - 2\lambda L^2\cosh u_*\sinh u_* = 0 \tag{A.12}$$

Substituting

$$\frac{dv_*}{du_*} = \frac{L\sinh u_*}{R\sinh v_*} \tag{A.13}$$

which follows from (A.10), we get:

$$\sinh u_*\big(\sinh u_* + \sinh v_* - 8\pi G\lambda L\cosh u_*\big) = 0. \tag{A.14}$$

Setting $u_* = 0$ is not a solution of the equations of motion; rather, it signals a breakdown of u_* as a collective coordinate. Equating the other factor of (A.14) to zero gives the second Israel junction condition, which is the second equality in (4.11).

To check the stability of the solution, we compute:

$$\left.\frac{d^2S}{du_*^2}\right|_{\text{EOM}} = 2\lambda L^2\,\frac{\sinh u_*}{\sinh v_*}\,. \tag{A.15}$$

Thus, stability requires that the product of λ, u_* and v_* must be positive. Excluding negative tensions leaves out $u_*, v_* < 0$ ($\lambda > 0$ forbids this by the equation of motion) and $u_*, v_* > 0$, i.e. $\alpha, \beta > \pi/2$. This is the only consistent, stable configuration.

A.2 Geodesics in the Thin Wall Geometry

It is interesting to find the geodesics of the thin wall geometry explicitly. We denote the endpoints of the geodesic with a, b and assume $a > b$.

Geodesics in the presence of a stable thin wall The stable configuration has $\alpha, \beta > \pi/2$. Geodesics that begin and end on the same side of the wall are same as in pure AdS_3. Their lengths are

$$S(a, b) = 2L \log \frac{a - b}{\mu}, \tag{A.16}$$

where μ is a large scale cutoff in the geometry. In the following we will drop the cutoffs, which in three bulk dimensions are simple additive constants.

To find the geodesics crossing the wall ($b < 0 < a$), observe that the geodesic motion in the hyperbolic plane is analogous to the propagation of a light ray in a medium whose index of refraction is $n(z) = L/z$. Due to the first Israel junction condition, the index of refraction at the brane is continuous. Thus, by Snell's law, a geodesic crossing the brane consists of two circular arcs, which meet at the location on the brane where no refraction occurs. The angles can be read off directly from the x-z plane, which is conformal to the geometry. Thus, we are looking for two arcs which meet the wall at the same location and the same angle in the x-z plane. One such a geodesic is plotted in figure A.1.

Finding this location is a simple minimization exercise. Consider a family of piece-wise geodesic curves, each of which consists of two circular arcs meeting at an arbitrary junction on the brane. Let $y = \sqrt{x^2 + z^2}$ be the coordinate distance of the junction from the defect; note that y-values on the two sides of the wall agree. One

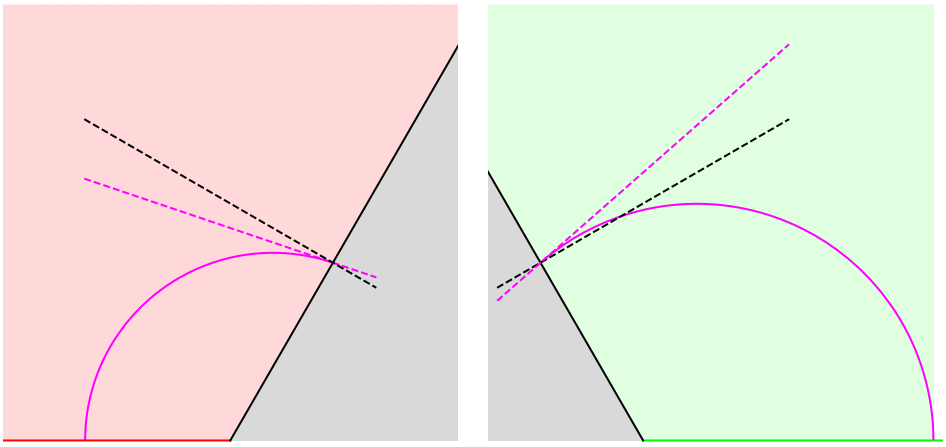

Figure A.1: A wall-crossing geodesic in a thin wall geometry consists of two arcs, which meet the wall at the same angle and location.

can easily write down the length of such a curve as a function of y:

$$S(\alpha,\beta,a,b,y) = L\log\left(\frac{b^2+y^2-2|b|y\cos\beta}{y\sin\beta}\right)+R\log\left(\frac{a^2+y^2-2ay\cos\alpha}{y\sin\alpha}\right) \quad \text{(A.17)}$$

To find the actual geodesic among this family of curves, we minimize the length formula above with respect to y. The critical value of y, which we denote y_*, is given by:

$$y_* = \frac{1}{2}\csc\left(\frac{\alpha+\beta}{2}\right)\left[(a-|b|)\sin\left(\frac{\beta-\alpha}{2}\right)+\sqrt{(a+|b|)^2\sin^2\left(\frac{\beta-\alpha}{2}\right)+4a|b|\sin\alpha\sin\beta}\right]. \quad \text{(A.18)}$$

Substituting this expression in (A.17) gives the desired geodesic length. For the kinematic space metric component, we would then take the second partial with respect to a and b as in eq. (4.12). We do not give the full expression here because it is not illuminating.

Negative wall tension and strong subadditivity The pathological case when both $\alpha,\beta < \pi/2$ has some further exotic properties. Geodesics corresponding to

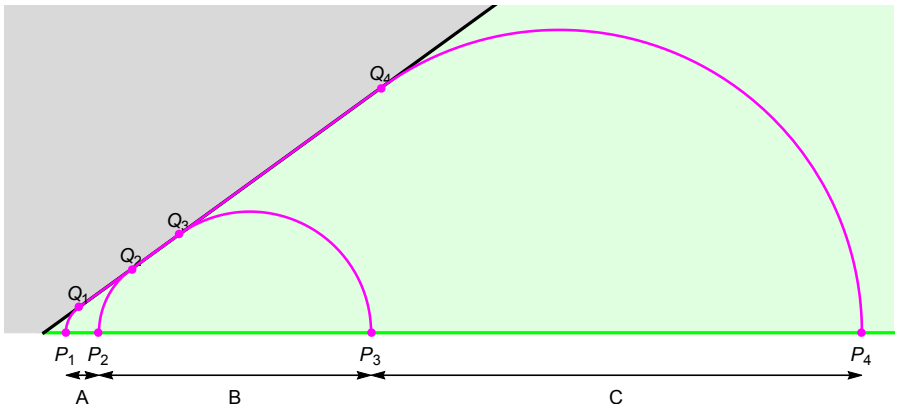

Figure A.2: Illustration of SSA saturation for squashed geodesics. A family of squashed geodesics spanning three adjacent boundary intervals.

regions with ξ greater than a certain critical value are 'squashed' by the wall: they consist of two semi-circular arcs that are tangent to the wall plus a finite segment along the wall. A family of such geodesics spanning three adjacent boundary intervals are depicted in figure A.2.

If we assume that this geometry obeys the Ryu-Takayanagi proposal for some dual CFT state, we immediately see that intervals depicted in figure A.2 saturate the strong subadditivity (SSA) of entanglement entropy. In kinematic space, SSA saturation results in a degenerate metric in certain wedge-shaped regions near the edges of the defect's causal cone. Saturation of SSA places a strong constraint on the entanglement structure of a quantum state [228]. Saturating it over a continuous family of intervals in a field theory is a powerful constraint, even if it is subject to $\mathcal{O}(1/N)$ corrections. It would be interesting to prove that such a set-up cannot be realized in a real CFT.

A.3 Kinematic Space of the Janus Solution

In this appendix, we compute the entanglement entropy and kinematic space of the Janus solution perturbatively for small γ^2. On a constant time slice of the Janus solution, expanding the metric (4.14-4.16) to first non-trivial order in γ gives:

$$ds^2 = L^2 \left(\cosh^2 u - \frac{\gamma^2}{2} \cosh 2u \right) dr^2 + L^2 du^2 \tag{A.19}$$

Applying the coordinate change (A.3) brings this metric to the form:

$$ds^2 = L^2 \frac{dx^2 + dz^2}{z^2} - \gamma^2 L^2 \frac{(z^2 + 2x^2)}{2z^2(x^2 + z^2)^2} (xdx + zdz)^2 \tag{A.20}$$

Perturbations of geodesic lengths generally arise from two effects: the shift in the metric and the shift in the coordinate trajectory of the geodesic. To lowest order, however, we can ignore the latter and only consider the former. Thus, we will take the geodesics to be semi-circles in the x-z plane. The perturbed induced metric on the semi-circle, which connects $u = x_0 - R$ and $v = x_0 + R$ takes the form:

$$ds^2 = L^2 \left[\frac{R^2}{(R^2 - (x - x_0)^2)^2} - \gamma^2 \frac{x_0^2 (R^2 + x^2 + 2xx_0 - x_0^2)}{2(R^2 + 2xx_0 - x_0^2)^2 (R^2 - x^2 + 2xx_0 - x_0^2)} \right] dx^2 \tag{A.21}$$

The perturbation of the length is:

$$\delta S = \frac{1}{2} \int \sqrt{g_{xx}} g^{xx} \delta g_{xx} dx \tag{A.22}$$

Evaluating the integral gives:

$$\begin{aligned} \delta S(R, x_0) &= -\gamma^2 \frac{L x_0^2}{2R} \int_{x_0 - R}^{x_0 + R} \frac{R^2 + x^2 + 2xx_0 - x_0^2}{(R^2 + 2xx_0 - x_0^2)^2} dx \\ &= -\frac{\gamma^2 L}{8Rx_0} \left(4Rx_0 + 2(R^2 - 3x_0^2) \log \left| \frac{R - x_0}{R + x_0} \right| \right) \end{aligned} \tag{A.23}$$

The correction to the kinematic space metric due to γ is then found by differentiation of δS:

$$\begin{aligned}\frac{\partial^2}{\partial u \partial v}\delta S &= \frac{1}{4}\left(\frac{\partial^2}{\partial x_0^2} - \frac{\partial^2}{\partial R^2}\right)\delta S \\ &= -\frac{\gamma^2 L}{16 R^3 x_0^3}\left(4Rx_0(R^2+3x_0^2) + 2(R^4+3x_0^4)\log\left|\frac{R-x_0}{R+x_0}\right|\right) \quad \text{(A.24)}\end{aligned}$$

This is eq. (4.18) from the main text.

Bibliography

[1] A. Manalaysay. **IDM2016**, http://luxdarkmatter.org/LUX_dark_matter/Talks_files/LUX_NewDarkMatterSearchResult_332LiveDays_IDM2016_160721.pdf . xii, 37, 38

[2] **LUX** Collaboration, D. S. Akerib et al., *Improved Limits on Scattering of Weakly Interacting Massive Particles from Reanalysis of 2013 LUX Data*, *Phys. Rev. Lett.* **116** (2016), no. 16 161301, [arXiv:1512.03506]. xii, 37, 38

[3] **SuperCDMS** Collaboration, R. Agnese et al., *New Results from the Search for Low-Mass Weakly Interacting Massive Particles with the CDMS Low Ionization Threshold Experiment*, *Phys. Rev. Lett.* **116** (2016), no. 7 071301, [arXiv:1509.02448]. xii, 37, 38

[4] **CRESST** Collaboration, G. Angloher et al., *Results on light dark matter particles with a low-threshold CRESST-II detector*, *Eur. Phys. J.* **C76** (2016), no. 1 25, [arXiv:1509.01515]. xii, 37, 38

[5] **Planck** Collaboration, P. A. R. Ade et al., *Planck 2015 results. XIII. Cosmological parameters*, *Astron. Astrophys.* **594** (2016) A13, [arXiv:1502.01589]. xii, 5, 35, 37, 38

[6] **Fermi-LAT** Collaboration, M. Ackermann et al., *Searching for Dark Matter Annihilation from Milky Way Dwarf Spheroidal Galaxies with Six Years of*

Fermi Large Area Telescope Data, *Phys. Rev. Lett.* **115** (2015), no. 23 231301, [arXiv:1503.02641]. xii, 37, 38

[7] **AMS** Collaboration, L. Accardo et al., *High Statistics Measurement of the Positron Fraction in Primary Cosmic Rays of 0.5500 GeV with the Alpha Magnetic Spectrometer on the International Space Station*, *Phys. Rev. Lett.* **113** (2014) 121101. xii, 37, 38

[8] **AMS** Collaboration, M. Aguilar et al., *Electron and Positron Fluxes in Primary Cosmic Rays Measured with the Alpha Magnetic Spectrometer on the International Space Station*, *Phys. Rev. Lett.* **113** (2014) 121102. xii, 37, 38

[9] G. Steigman, B. Dasgupta, and J. F. Beacom, *Precise Relic WIMP Abundance and its Impact on Searches for Dark Matter Annihilation*, *Phys. Rev.* **D86** (2012) 023506, [arXiv:1204.3622]. xii, 38

[10] **CMS** Collaboration, S. Chatrchyan et al., *Observation of a new boson at a mass of 125 GeV with the CMS experiment at the LHC*, *Phys. Lett.* **B716** (2012) 30–61, [arXiv:1207.7235]. 1, 4

[11] **ATLAS** Collaboration, G. Aad et al., *Observation of a new particle in the search for the Standard Model Higgs boson with the ATLAS detector at the LHC*, *Phys. Lett.* **B716** (2012) 1–29, [arXiv:1207.7214]. 1, 4

[12] J. M. Maldacena, *The Large N limit of superconformal field theories and supergravity*, *Int. J. Theor. Phys.* **38** (1999) 1113–1133, [hep-th/9711200]. [Adv. Theor. Math. Phys.2,231(1998)]. 2

[13] E. Witten, *Anti-de Sitter space and holography*, *Adv. Theor. Math. Phys.* **2** (1998) 253–291, [hep-th/9802150]. 2

[14] O. Aharony, S. S. Gubser, J. M. Maldacena, H. Ooguri, and Y. Oz, *Large N field theories, string theory and gravity*, *Phys. Rept.* **323** (2000) 183–386, [hep-th/9905111]. 2

[15] **Planck** Collaboration, R. Adam et al., *Planck 2015 results. I. Overview of products and scientific results*, *Astron. Astrophys.* **594** (2016) A1, [arXiv:1502.01582]. 5

[16] S. Nussinov, *TECHNOCOSMOLOGY: COULD A TECHNIBARYON EXCESS PROVIDE A 'NATURAL' MISSING MASS CANDIDATE?*, *Phys. Lett.* **B165** (1985) 55–58. 6, 29

[17] G. B. Gelmini, L. J. Hall, and M. J. Lin, *What Is the Cosmion?*, *Nucl. Phys.* **B281** (1987) 726. 6, 29

[18] S. M. Barr, R. S. Chivukula, and E. Farhi, *Electroweak Fermion Number Violation and the Production of Stable Particles in the Early Universe*, *Phys. Lett.* **B241** (1990) 387–391. 6, 29

[19] S. M. Barr, *Baryogenesis, sphalerons and the cogeneration of dark matter*, *Phys. Rev.* **D44** (1991) 3062–3066. 6, 29

[20] D. B. Kaplan, *A Single explanation for both the baryon and dark matter densities*, *Phys. Rev. Lett.* **68** (1992) 741–743. 6, 29

[21] D. E. Kaplan, M. A. Luty, and K. M. Zurek, *Asymmetric Dark Matter*, *Phys. Rev.* **D79** (2009) 115016, [arXiv:0901.4117]. 6, 29

[22] K. Petraki and R. R. Volkas, *Review of asymmetric dark matter*, *Int. J. Mod. Phys.* **A28** (2013) 1330028, [arXiv:1305.4939]. 6, 29

[23] K. M. Zurek, *Asymmetric Dark Matter: Theories, Signatures, and Constraints*, *Phys. Rept.* **537** (2014) 91–121, [arXiv:1308.0338]. 6, 29

[24] C. Kilic and S. Swaminathan, *Can A Pseudo-Nambu-Goldstone Higgs Lead To Symmetry Non-Restoration?*, *JHEP* **01** (2016) 002, [arXiv:1508.05121]. 8

[25] D. A. Kirzhnits and A. D. Linde, *Macroscopic Consequences of the Weinberg Model*, *Phys. Lett.* **B42** (1972) 471–474. 8

[26] D. A. Kirzhnits and A. D. Linde, *A Relativistic phase transition*, *Sov. Phys. JETP* **40** (1975) 628. [Zh. Eksp. Teor. Fiz.67,1263(1974)]. 8

[27] D. A. Kirzhnits and A. D. Linde, *Symmetry Behavior in Gauge Theories*, *Annals Phys.* **101** (1976) 195–238. 8

[28] M. E. Carrington, *The Effective potential at finite temperature in the Standard Model*, *Phys. Rev.* **D45** (1992) 2933–2944. 8

[29] P. B. Arnold and O. Espinosa, *The Effective potential and first order phase transitions: Beyond leading-order*, *Phys. Rev.* **D47** (1993) 3546, [hep-ph/9212235]. [Erratum: Phys. Rev.D50,6662(1994)]. 8

[30] J. R. Espinosa, M. Quiros, and F. Zwirner, *On the nature of the electroweak phase transition*, *Phys. Lett.* **B314** (1993) 206–216, [hep-ph/9212248]. 8

[31] J. R. Espinosa, M. Losada, and A. Riotto, *Symmetry nonrestoration at high temperature in little Higgs models*, *Phys. Rev.* **D72** (2005) 043520, [hep-ph/0409070]. 8, 9, 26

[32] S. Aziz, B. Ghosh, and G. Dey, *Broken electroweak phase at high temperature in the Littlest Higgs model with T-parity*, *Phys. Rev.* **D79** (2009) 075001, [arXiv:0901.3442]. 8

[33] A. Ahriche, *The Restoration of the Electroweak Symmetry at High Temperature for Little Higgs*, arXiv:1003.5045. 8

[34] N. Arkani-Hamed, A. G. Cohen, and H. Georgi, *(De)constructing dimensions*, *Phys. Rev. Lett.* **86** (2001) 4757–4761, [hep-th/0104005]. 9

[35] N. Arkani-Hamed, A. G. Cohen, and H. Georgi, *Electroweak symmetry breaking from dimensional deconstruction*, *Phys. Lett.* **B513** (2001) 232–240, [hep-ph/0105239]. 9

[36] N. Arkani-Hamed, A. G. Cohen, T. Gregoire, and J. G. Wacker, *Phenomenology of electroweak symmetry breaking from theory space*, *JHEP* **08** (2002) 020, [hep-ph/0202089]. 9

[37] N. Arkani-Hamed, A. G. Cohen, E. Katz, A. E. Nelson, T. Gregoire, and J. G. Wacker, *The Minimal moose for a little Higgs*, *JHEP* **08** (2002) 021, [hep-ph/0206020]. 9

[38] N. Arkani-Hamed, A. G. Cohen, E. Katz, and A. E. Nelson, *The Littlest Higgs*, *JHEP* **07** (2002) 034, [hep-ph/0206021]. 9

[39] S. Weinberg, *Gauge and Global Symmetries at High Temperature*, *Phys. Rev.* **D9** (1974) 3357–3378. 9, 21

[40] R. N. Mohapatra and G. Senjanovic, *Soft CP Violation at High Temperature*, *Phys. Rev. Lett.* **42** (1979) 1651. 9

[41] R. N. Mohapatra and G. Senjanovic, *Broken Symmetries at High Temperature*, *Phys. Rev.* **D20** (1979) 3390–3398. 9

[42] J. R. Espinosa and J. M. No, *Scalar loops in little Higgs models*, *JHEP* **01** (2007) 006, [hep-ph/0610255]. 9

[43] Z. Chacko, H.-S. Goh, and R. Harnik, *The Twin Higgs: Natural electroweak breaking from mirror symmetry*, *Phys. Rev. Lett.* **96** (2006) 231802, [hep-ph/0506256]. 9, 10

[44] R. Barbieri, T. Gregoire, and L. J. Hall, *Mirror world at the large hadron collider*, hep-ph/0509242. 10

[45] Z. Chacko, Y. Nomura, M. Papucci, and G. Perez, *Natural little hierarchy from a partially goldstone twin Higgs*, *JHEP* **01** (2006) 126, [hep-ph/0510273]. 10

[46] Z. Chacko, H.-S. Goh, and R. Harnik, *A Twin Higgs model from left-right symmetry*, *JHEP* **01** (2006) 108, [hep-ph/0512088]. 10

[47] R. Foot and R. R. Volkas, *Natural electroweak symmetry breaking in generalised mirror matter models*, *Phys. Lett.* **B645** (2007) 75–81, [hep-ph/0610013]. 10

[48] H.-S. Goh and C. A. Krenke, *A Little Twin Higgs Model*, *Phys. Rev.* **D76** (2007) 115018, [arXiv:0707.3650]. 10

[49] N. Craig, S. Knapen, and P. Longhi, *Neutral Naturalness from Orbifold Higgs Models*, *Phys. Rev. Lett.* **114** (2015), no. 6 061803, [arXiv:1410.6808]. 10

[50] M. Geller and O. Telem, *Holographic Twin Higgs Model*, *Phys. Rev. Lett.* **114** (2015), no. 19 191801, [arXiv:1411.2974]. 10

[51] R. Barbieri, D. Greco, R. Rattazzi, and A. Wulzer, *The Composite Twin Higgs scenario*, arXiv:1501.07803. 10

[52] M. Low, A. Tesi, and L.-T. Wang, *Twin Higgs mechanism and a composite Higgs boson*, *Phys. Rev.* **D91** (2015) 095012, [arXiv:1501.07890]. 10

[53] N. Craig, A. Katz, M. Strassler, and R. Sundrum, *Naturalness in the Dark at the LHC*, arXiv:1501.05310. 10

[54] H.-S. Goh and S. Su, *Phenomenology of The Left-Right Twin Higgs Model*, *Phys. Rev.* **D75** (2007) 075010, [hep-ph/0611015]. 11, 14

[55] D.-W. Jung and J. Y. Lee, *One-loop Radiative Corrections to the ρ Parameter in the Left Right Twin Higgs Model*, *J. Korean Phys. Soc.* **63** (2013), no. 6 1114–1127, [hep-ph/0701071]. 11, 14

[56] A. Abada and I. Hidalgo, *Neutrinos and lepton flavour violation in the left-right twin Higgs model*, *Phys. Rev.* **D77** (2008) 113013, [arXiv:0711.1238]. 11, 14

[57] E. M. Dolle and S. Su, *Dark Matter in the Left Right Twin Higgs Model*, *Phys. Rev.* **D77** (2008) 075013, [arXiv:0712.1234]. 11, 14

[58] P. Batra and Z. Chacko, *A Composite Twin Higgs Model*, *Phys. Rev.* **D79** (2009) 095012, [arXiv:0811.0394]. 11, 14

[59] Y.-B. Liu, X.-L. Wang, H.-M. Han, and Y.-H. Cao, *Single production of charged gauge boson W_H - from left-right twin Higgs model in association with top quark at LHC*, *Commun. Theor. Phys.* **49** (2008) 977–980. 11, 14

[60] Y.-B. Liu, X.-L. Wang, J. Cao, and H.-M. Han, *Single production of top quark via e- gamma collision in left-right twin Higgs model*, *Commun. Theor. Phys.* **50** (2008) 445–450. 11, 14

[61] Y.-B. Liu, X.-L. Wang, and H.-M. Han, *The Higgs-strahlung and double Higgs-strahlung production in the left-right twin Higgs model at the ILC*, *Europhys. Lett.* **81** (2008) 31001. 11, 14

[62] Y.-B. Liu and S.-W. Wang, *Left-right twin Higgs model and the spin correction of top-quark pair production at ILC*, *Int. J. Mod. Phys.* **A24** (2009) 4261–4270. 11, 14

[63] W. Ma, C.-X. Yue, and Y.-Z. Wang, *Pair production of neutral Higgs bosons from the left-right twin Higgs model at the ILC and LHC*, *Phys. Rev.* **D79** (2009) 095010, [arXiv:0905.0597]. 11, 14

[64] Y.-B. Liu, L.-L. Du, and Q. Chang, *Probing new gauge boson Z-prime from the left-right twin Higgs model at high-energy e+ e- colliders*, *Mod. Phys. Lett.* **A24** (2009) 463–473. 11, 14

[65] H.-S. Goh and C. A. Krenke, *Lepton Number Violating Signals of the Top Partners in the Left-Right Twin Higgs Model*, *Phys. Rev.* **D81** (2010) 055008, [arXiv:0911.5567]. 11, 14

[66] J.-F. Shen, Y.-B. Liu, H. Zhao, and J. Cao, *Production of charged Higgs bosons from left-right twin Higgs model at TeV energy e- gamma colliders*, *Commun. Theor. Phys.* **54** (2010) 701–708. 11, 14

[67] Y.-B. Liu and X.-L. Wang, *Pair production of Higgs bosons associated with Z boson in the left-right twin Higgs model at the ILC*, *Nucl. Phys.* **B839** (2010) 294–309, [arXiv:1006.4589]. 11, 14

[68] Y.-B. Liu and X.-L. Wang, *Higgs boson decays and production in the left-right twin Higgs model*, *Phys. Lett.* **B694** (2011) 417–423, [arXiv:1010.4198]. 11, 14

[69] J.-F. Shen and Y.-B. Liu, *Production of h t anti-t and h t anti-T in the left-right twin Higgs model in gamma gamma collisions at ILC*, *Int. J. Mod. Phys.* **A26** (2011) 5133–5142. 11, 14

[70] J.-F. Shen, X.-M. Cui, Y.-Q. Li, and Y.-H. Gao, *Single production of a heavy T-quark in the left-right twin Higgs model at LHeC*, *Chin. Phys. Lett.* **28** (2011) 111203. 11, 14

[71] Y.-J. Zhang and G.-R. Lu, *Associated ZH and WH production in left-right twin Higgs model at LHC*, *Commun. Theor. Phys.* **56** (2011) 119–124. 11, 14

[72] L. Wang and X.-F. Han, *Light Higgs decay modes of Z-boson in the left-right twin Higgs model*, *Nucl. Phys.* **B850** (2011) 233–241. 11, 14

[73] W. Ma, C.-X. Yue, and T.-T. Zhang, *Pair production of neutral Higgs bosons from the left-right twin Higgs model via gamma gamma collisions*, *Chin. Phys.* **C35** (2011) 333–338. 11, 14

[74] L. Wang and X.-F. Han, *Standard-model-like Higgs-pair production and decay in left-right twin Higgs model*, *Phys. Lett.* **B696** (2011) 79–86. 11, 14

[75] Y.-B. Liu, *Pseudoscalar boson and SM-like Higgs boson production at ILC in the left-right twin Higgs model*, *Phys. Lett.* **B698** (2011) 157–161. 11, 14

[76] L. Wang, L. Wu, and J. M. Yang, *Top quark forward-backward asymmetry and charge asymmetry in left-right twin Higgs model*, *Phys. Rev.* **D85** (2012) 075017, [arXiv:1111.4771]. 11, 14

[77] Z.-Y. Guo, G. Yang, and B.-F. Yang, *Single vector-like top partner production in the Left-Right Twin Higgs model at TeV energy $e\gamma$ colliders*, *Chin.Phys.* **C37** (2013), no. 10 103101, [arXiv:1304.2249]. 11, 14

[78] Y.-B. Liu, S. Cheng, and Z.-J. Xiao, *Left-right twin Higgs model confronted with the latest LHC Higgs data*, *Phys. Rev.* **D89** (2014), no. 1 015013, [arXiv:1311.0183]. 11, 14

[79] Y.-B. Liu and Z.-J. Xiao, *Production and decays of a light ϕ^0 in the LRTH model under the LHC Higgs data*, *JHEP* **02** (2014) 128, [arXiv:1312.4004]. 11, 14

[80] J. Han, B. Yang, and X. Zhang, *Associated production of the Z boson with a pair of top quarks in the left-right twin Higgs model*, *Europhys. Lett.* **105** (2014) 31001, [arXiv:1401.3594]. 11, 14

[81] Y.-B. Liu and Z.-J. Xiao, *The production and decay of the top partner T in the leftright twin Higgs model at the ILC and CLIC*, *Nucl. Phys.* **B892** (2015) 63–82, [arXiv:1409.6050]. 11, 14

[82] Y.-B. Liu and Z.-J. Xiao, *Constraining dark matter in the LRTH model with latest LHC, XENON100 and LUX data*, *J. Phys.* **G42** (2015), no. 5 055004, [arXiv:1409.8000]. 11, 14

[83] G. Burdman, Z. Chacko, R. Harnik, L. de Lima, and C. B. Verhaaren, *Colorless Top Partners, a 125 GeV Higgs, and the Limits on Naturalness*, *Phys. Rev.* **D91** (2015), no. 5 055007, [arXiv:1411.3310]. 11, 14

[84] N. Craig, S. Knapen, and P. Longhi, *The Orbifold Higgs*, *JHEP* **03** (2015) 106, [arXiv:1411.7393]. 11, 14

[85] Y.-B. Liu and Z.-J. Xiao, *Single Higgs boson production at the ILC in the left-right twin Higgs model*, *J. Phys.* **G42** (2015), no. 6 065005, [arXiv:1412.5905]. 11, 14

[86] J. Hetzel and B. Stech, *Low-energy phenomenology of trinification: an effective left-right-symmetric model*, *Phys. Rev.* **D91** (2015) 055026, [arXiv:1502.00919]. 11, 14

[87] P. Schwaller, *Gravitational Waves From a Dark (Twin) Phase Transition*, arXiv:1504.07263. 11, 14

[88] J. Han, S. Li, B. Yang, and N. Liu, *Higgs boson production and decay at e^+e^- colliders as a probe of the Left-Right twin Higgs model*, *Nucl. Phys.* **B896** (2015) 200–211, [arXiv:1504.08236]. 11, 14

[89] I. Garca Garca, R. Lasenby, and J. March-Russell, *Twin Higgs WIMP Dark Matter*, arXiv:1505.07109. 11, 14

[90] N. Craig and A. Katz, *The Fraternal WIMP Miracle*, arXiv:1505.07113. 11, 14

[91] I. Garca Garca, R. Lasenby, and J. March-Russell, *Twin Higgs Asymmetric Dark Matter*, arXiv:1505.07410. 11, 14

[92] M. Farina, *Asymmetric Twin Dark Matter*, arXiv:1506.03520. 11, 14

[93] D. Curtin and C. B. Verhaaren, *Discovering Uncolored Naturalness in Exotic Higgs Decays*, arXiv:1506.06141. 11, 14

[94] L. Dolan and R. Jackiw, *Symmetry Behavior at Finite Temperature*, *Phys. Rev.* **D9** (1974) 3320–3341. 15

[95] J. I. Kapusta and C. Gale, *Finite-temperature field theory: Principles and applications*. Cambridge University Press, 2011. 15

[96] N. K. Nielsen, *On the Gauge Dependence of Spontaneous Symmetry Breaking in Gauge Theories*, *Nucl. Phys.* **B101** (1975) 173. 16

[97] H. H. Patel and M. J. Ramsey-Musolf, *Baryon Washout, Electroweak Phase Transition, and Perturbation Theory*, *JHEP* **07** (2011) 029, [arXiv:1101.4665]. 16

[98] A. Andreassen, W. Frost, and M. D. Schwartz, *Consistent Use of Effective Potentials*, *Phys. Rev.* **D91** (2015), no. 1 016009, [arXiv:1408.0287]. 16

[99] D. Comelli and J. R. Espinosa, *Bosonic thermal masses in supersymmetry*, *Phys. Rev.* **D55** (1997) 6253–6263, [hep-ph/9606438]. 18

[100] M. Sakamoto and K. Takenaga, *On Gauge Symmetry Breaking via Euclidean Time Component of Gauge Fields*, *Phys. Rev.* **D76** (2007) 085016, [arXiv:0706.0071]. 20

[101] C. Delaunay, C. Grojean, and J. D. Wells, *Dynamics of Non-renormalizable Electroweak Symmetry Breaking*, *JHEP* **04** (2008) 029, [arXiv:0711.2511]. 20

[102] A. D. Linde, *Infrared Problem in Thermodynamics of the Yang-Mills Gas*, *Phys. Lett.* **B96** (1980) 289. 21

[103] K. Kajantie, M. Laine, K. Rummukainen, and M. E. Shaposhnikov, *Is there a hot electroweak phase transition at m(H) larger or equal to m(W)?*, *Phys. Rev. Lett.* **77** (1996) 2887–2890, [hep-ph/9605288]. 21

[104] D. E. Morrissey and M. J. Ramsey-Musolf, *Electroweak baryogenesis*, *New J. Phys.* **14** (2012) 125003, [arXiv:1206.2942]. 21

[105] P. B. Arnold, *The Electroweak phase transition: Part 1. Review of perturbative methods*, in *International Seminar: Quarks - 94 Vladimir, Russia, May 11-18, 1994*, 1994. hep-ph/9410294. 21

[106] G. Panico and M. Serone, *The Electroweak phase transition on orbifolds with gauge-Higgs unification*, *JHEP* **05** (2005) 024, [hep-ph/0502255]. 27

[107] P. W. Graham, D. E. Kaplan, and S. Rajendran, *Cosmological Relaxation of the Electroweak Scale*, arXiv:1504.07551. 27

[108] J. Orloff, *The UV price for symmetry nonrestoration*, *Phys. Lett.* **B403** (1997) 309–315, [hep-ph/9611398]. 28

[109] A. D. Linde, *High Density and High Temperature Symmetry Behavior in Gauge Theories*, *Phys. Rev.* **D14** (1976) 3345. 28

[110] H. E. Haber and H. A. Weldon, *Finite Temperature Symmetry Breaking as Bose-Einstein Condensation*, *Phys. Rev.* **D25** (1982) 502. 28

[111] K. M. Benson, J. Bernstein, and S. Dodelson, *Phase structure and the effective potential at fixed charge*, *Phys. Rev.* **D44** (1991) 2480–2497. 28

[112] A. Riotto and G. Senjanovic, *Supersymmetry and broken symmetries at high temperature*, *Phys. Rev. Lett.* **79** (1997) 349–352, [hep-ph/9702319]. 28

[113] P. Agrawal, C. Kilic, S. Swaminathan, and C. Trendafilova, *Secretly Asymmetric Dark Matter*, *Phys. Rev.* **D95** (2017), no. 1 015031, [arXiv:1608.04745]. 29

[114] A. Falkowski, J. T. Ruderman, and T. Volansky, *Asymmetric Dark Matter from Leptogenesis*, *JHEP* **05** (2011) 106, [arXiv:1101.4936]. 29

[115] E. Hardy, R. Lasenby, and J. Unwin, *Annihilation Signals from Asymmetric Dark Matter*, *JHEP* **07** (2014) 049, [arXiv:1402.4500]. 29

[116] M. R. Buckley and S. Profumo, *Regenerating a Symmetry in Asymmetric Dark Matter*, *Phys. Rev. Lett.* **108** (2012) 011301, [arXiv:1109.2164]. 29

[117] M. Cirelli, P. Panci, G. Servant, and G. Zaharijas, *Consequences of DM/antiDM Oscillations for Asymmetric WIMP Dark Matter*, *JCAP* **1203** (2012) 015, [arXiv:1110.3809]. 29

[118] S. Tulin, H.-B. Yu, and K. M. Zurek, *Oscillating Asymmetric Dark Matter*, *JCAP* **1205** (2012) 013, [arXiv:1202.0283]. 29

[119] N. Okada and O. Seto, *Originally Asymmetric Dark Matter*, *Phys. Rev.* **D86** (2012) 063525, [arXiv:1205.2844]. 29

[120] S.-L. Chen and Z. Kang, *Oscillating Asymmetric Sneutrino Dark Matter from the Maximally $U(1)_L$ Supersymmetric Inverse Seesaw*, arXiv:1512.08780. 29

[121] J. March-Russell, C. McCabe, and M. McCullough, *Neutrino-Flavoured Sneutrino Dark Matter*, *JHEP* **03** (2010) 108, [arXiv:0911.4489]. 30

[122] B. Batell, J. Pradler, and M. Spannowsky, *Dark Matter from Minimal Flavor Violation*, *JHEP* **08** (2011) 038, [arXiv:1105.1781]. 30

[123] P. Agrawal, S. Blanchet, Z. Chacko, and C. Kilic, *Flavored Dark Matter, and Its Implications for Direct Detection and Colliders*, *Phys. Rev.* **D86** (2012) 055002, [arXiv:1109.3516]. 30

[124] J. Kile, *Flavored Dark Matter: A Review*, *Mod. Phys. Lett.* **A28** (2013) 1330031, [arXiv:1308.0584]. 30

[125] A. Kumar and S. Tulin, *Top-flavored dark matter and the forward-backward asymmetry*, *Phys. Rev.* **D87** (2013), no. 9 095006, [arXiv:1303.0332]. 30

[126] L. Lopez-Honorez and L. Merlo, *Dark matter within the minimal flavour violation ansatz*, *Phys. Lett.* **B722** (2013) 135–143, [arXiv:1303.1087]. 30

[127] B. Batell, T. Lin, and L.-T. Wang, *Flavored Dark Matter and R-Parity Violation*, *JHEP* **01** (2014) 075, [arXiv:1309.4462]. 30

[128] P. Agrawal, B. Batell, D. Hooper, and T. Lin, *Flavored Dark Matter and the Galactic Center Gamma-Ray Excess*, *Phys. Rev.* **D90** (2014), no. 6 063512, [arXiv:1404.1373]. 30

[129] P. Agrawal, M. Blanke, and K. Gemmler, *Flavored dark matter beyond Minimal Flavor Violation*, *JHEP* **10** (2014) 72, [arXiv:1405.6709]. 30

[130] A. Hamze, C. Kilic, J. Koeller, C. Trendafilova, and J.-H. Yu, *Lepton-Flavored Asymmetric Dark Matter and Interference in Direct Detection*, *Phys. Rev.* **D91** (2015), no. 3 035009, [arXiv:1410.3030]. 30

[131] C.-J. Lee and J. Tandean, *Lepton-Flavored Scalar Dark Matter with Minimal Flavor Violation*, *JHEP* **04** (2015) 174, [arXiv:1410.6803]. 30

[132] C. Kilic, M. D. Klimek, and J.-H. Yu, *Signatures of Top Flavored Dark Matter*, *Phys. Rev.* **D91** (2015), no. 5 054036, [arXiv:1501.02202]. 30

[133] F. Bishara, A. Greljo, J. F. Kamenik, E. Stamou, and J. Zupan, *Dark Matter and Gauged Flavor Symmetries*, *JHEP* **12** (2015) 130, [arXiv:1505.03862]. 30

[134] B. Bhattacharya, D. London, J. M. Cline, A. Datta, and G. Dupuis, *Quark-flavored scalar dark matter*, *Phys. Rev.* **D92** (2015), no. 11 115012, [arXiv:1509.04271]. 30

[135] L. Calibbi, A. Crivellin, and B. Zaldvar, *Flavor portal to dark matter*, *Phys. Rev.* **D92** (2015), no. 1 016004, [arXiv:1501.07268]. 30

[136] S. Baek and Z.-F. Kang, *Naturally Large Radiative Lepton Flavor Violating Higgs Decay Mediated by Lepton-flavored Dark Matter*, *JHEP* **03** (2016) 106, [arXiv:1510.00100]. 30

[137] M.-C. Chen, J. Huang, and V. Takhistov, *Beyond Minimal Lepton Flavored Dark Matter*, *JHEP* **02** (2016) 060, [arXiv:1510.04694]. 30

[138] M. Fukugita and T. Yanagida, *Baryogenesis Without Grand Unification*, *Phys. Lett.* **B174** (1986) 45–47. 31

[139] S. Davidson, E. Nardi, and Y. Nir, *Leptogenesis*, *Phys. Rept.* **466** (2008) 105–177, [arXiv:0802.2962]. 31

[140] C. S. Fong, E. Nardi, and A. Riotto, *Leptogenesis in the Universe*, *Adv. High Energy Phys.* **2012** (2012) 158303, [arXiv:1301.3062]. 31

[141] J. March-Russell, H. Murayama, and A. Riotto, *The Small observed baryon asymmetry from a large lepton asymmetry*, *JHEP* **11** (1999) 015, [hep-ph/9908396]. 35

[142] P. Agrawal, Z. Chacko, C. Kilic, and C. B. Verhaaren, *A Couplet from Flavored Dark Matter*, *JHEP* **08** (2015) 072, [arXiv:1503.03057]. 35

[143] B. Holdom, *Two U(1)'s and Epsilon Charge Shifts*, *Phys. Lett.* **B166** (1986) 196–198. 37

[144] E. J. Chun, J.-C. Park, and S. Scopel, *Dark matter and a new gauge boson through kinetic mixing*, *JHEP* **02** (2011) 100, [arXiv:1011.3300]. 37

[145] N. Arkani-Hamed, D. P. Finkbeiner, T. R. Slatyer, and N. Weiner, *A Theory of Dark Matter*, *Phys. Rev.* **D79** (2009) 015014, [arXiv:0810.0713]. 37

[146] T. R. Slatyer, *Indirect dark matter signatures in the cosmic dark ages. I. Generalizing the bound on s-wave dark matter annihilation from Planck results*, *Phys. Rev.* **D93** (2016), no. 2 023527, [arXiv:1506.03811]. 37

[147] G. Elor, N. L. Rodd, T. R. Slatyer, and W. Xue, *Model-Independent Indirect Detection Constraints on Hidden Sector Dark Matter*, *JCAP* **1606** (2016), no. 06 024, [arXiv:1511.08787]. 37

[148] D. Curtin, R. Essig, S. Gori, and J. Shelton, *Illuminating Dark Photons with High-Energy Colliders*, *JHEP* **02** (2015) 157, [arXiv:1412.0018]. 39

[149] S. Alekhin et al., *A facility to Search for Hidden Particles at the CERN SPS: the SHiP physics case*, arXiv:1504.04855. 39

[150] B. Czech, P. H. Nguyen, and S. Swaminathan, *A defect in holographic interpretations of tensor networks*, *JHEP* **03** (2017) 090, [arXiv:1612.05698]. 41, 69

[151] J. Maldacena, *The Large-N Limit of Superconformal Field Theories and Supergravity*, *International Journal of Theoretical Physics* **38** (1999) 1113–1133, [hep-th/9711200]. 41

[152] E. Witten, *Anti-de Sitter space and holography*, *Advances in Theoretical and Mathematical Physics* **2** (1998) 253–291, [hep-th/9802150]. 41

[153] S. Ryu and T. Takayanagi, *Holographic Derivation of Entanglement Entropy from the anti de Sitter Space/Conformal Field Theory Correspondence*, *Physical Review Letters* **96** (May, 2006) 181602, [hep-th/0603001]. 41

[154] S. Ryu and T. Takayanagi, *Aspects of holographic entanglement entropy*, *Journal of High Energy Physics* **8** (Aug., 2006) 045, [hep-th/0605073]. 41

[155] G. Vidal, *Entanglement Renormalization*, *Physical Review Letters* **99** (Nov., 2007) 220405, [cond-mat/0512165]. 41, 56, 61

[156] G. Vidal, *Class of Quantum Many-Body States That Can Be Efficiently Simulated*, *Physical Review Letters* **101** (Sept., 2008) 110501, [quant-ph/0610099]. 41, 49

[157] B. Swingle, *Entanglement renormalization and holography*, Phys. Rev. D **86** (Sept., 2012) 065007, [arXiv:0905.1317]. 41, 43, 44, 56, 57, 60, 61, 68

[158] B. Swingle, *Constructing holographic spacetimes using entanglement renormalization*, *ArXiv e-prints* (Sept., 2012) [arXiv:1209.3304]. 41, 43

[159] X.-L. Qi, *Exact holographic mapping and emergent space-time geometry*, *ArXiv e-prints* (Sept., 2013) [arXiv:1309.6282]. 41

[160] M. Miyaji, T. Numasawa, N. Shiba, T. Takayanagi, and K. Watanabe, *Continuous Multiscale Entanglement Renormalization Ansatz as Holographic Surface-State Correspondence*, *Physical Review Letters* **115** (Oct., 2015) 171602, [arXiv:1507.07555]. 41

[161] C. H. Lee and X.-L. Qi, *Exact holographic mapping in free fermion systems*, Phys. Rev. B **93** (Jan., 2016) 035112, [arXiv:1503.08592]. 41

[162] M. Miyaji, T. Takayanagi, and K. Watanabe, *From path integrals to tensor networks for the AdS /CFT correspondence*, Phys. Rev. D **95** (Mar., 2017) 066004, [arXiv:1609.04645]. 41

[163] M. Han and L.-Y. Hung, *Loop quantum gravity, exact holographic mapping, and holographic entanglement entropy*, Phys. Rev. D **95** (Jan., 2017) 024011, [arXiv:1610.02134]. 41

[164] B. Czech, L. Lamprou, S. McCandlish, and J. Sully, *Integral geometry and holography*, *Journal of High Energy Physics* **10** (Oct., 2015) 175, [arXiv:1505.05515]. 41, 43, 45, 56, 62

[165] B. Czech, L. Lamprou, S. McCandlish, and J. Sully, *Tensor networks from kinematic space*, *Journal of High Energy Physics* **7** (July, 2016) 100, [arXiv:1512.01548]. 41, 42, 43, 44, 49, 56, 57, 60, 61, 62, 68

[166] B. Czech, G. Evenbly, L. Lamprou, S. McCandlish, X.-l. Qi, J. Sully, and G. Vidal. 41, 54, 56, 61, 67

[167] D. Marolf, H. Maxfield, A. Peach, and S. Ross, *Hot multiboundary wormholes from bipartite entanglement*, *Classical and Quantum Gravity* **32** (Nov., 2015) 215006, [arXiv:1506.04128]. 41

[168] J. Maldacena and L. Susskind, *Cool horizons for entangled black holes*, *Fortschritte der Physik* **61** (Sept., 2013) 781–811, [arXiv:1306.0533]. 42

[169] L. Susskind, *Butterflies on the Stretched Horizon*, *ArXiv e-prints* (Nov., 2013) [arXiv:1311.7379]. 42

[170] T. Hartman and J. Maldacena, *Time evolution of entanglement entropy from black hole interiors*, *Journal of High Energy Physics* **5** (May, 2013) 14, [arXiv:1303.1080]. 42

[171] D. A. Roberts, D. Stanford, and L. Susskind, *Localized shocks*, *Journal of High Energy Physics* **3** (Mar., 2015) 51, [arXiv:1409.8180]. 42

[172] L. Susskind, *Entanglement is not enough*, *Fortschritte der Physik* **64** (Jan., 2016) 49–71. 42

[173] P. Hosur, X.-L. Qi, D. A. Roberts, and B. Yoshida, *Chaos in quantum channels*, *Journal of High Energy Physics* **2** (Feb., 2016) 4, [arXiv:1511.04021]. 42

[174] A. R. Brown, D. A. Roberts, L. Susskind, B. Swingle, and Y. Zhao, *Complexity, action, and black holes*, Phys. Rev. D **93** (Apr., 2016) 086006, [arXiv:1512.04993]. 42

[175] V. Chua, V. Passias, A. Tiwari, and S. Ryu, *Holographic dynamics from multiscale entanglement renormalization ansatz*, Phys. Rev. B **95** (May, 2017) 195152, [arXiv:1611.05877]. 42

[176] A. May, *Tensor networks for dynamic spacetimes*, *ArXiv e-prints* (Nov., 2016) [arXiv:1611.06220]. 42

[177] S. Leutheusser and M. Van Raamsdonk, *Tensor Network Models of Unitary Black Hole Evaporation*, *ArXiv e-prints* (Nov., 2016) [arXiv:1611.08613]. 42

[178] G. Evenbly and G. Vidal, *Theory of minimal updates in holography*, Phys. Rev. B **91** (May, 2015) 205119. 42, 43, 48, 49, 50, 51, 53, 56, 67, 68

[179] A. Karch and L. Randall, *Open and closed string interpretation of SUSY CFT's on branes with boundaries*, *Journal of High Energy Physics* **6** (June, 2001) 063, [hep-th/0105132]. 42, 58

[180] O. Aharony, O. DeWolfe, D. Z. Freedman, and A. Karch, *Defect conformal field theory and locally localized gravity*, *Journal of High Energy Physics* **7** (July, 2003) 030, [hep-th/0303249]. 42, 58

[181] D. Bak, M. Gutperle, and S. Hirano, *Three dimensional Janus and time-dependent black holes*, *Journal of High Energy Physics* **2** (Feb., 2007) 068, [hep-th/0701108]. 42, 63, 65

[182] T. Takayanagi, *Holographic Dual of a Boundary Conformal Field Theory*, *Physical Review Letters* **107** (Sept., 2011) 101602, [arXiv:1105.5165]. 42, 58, 59

[183] M. Fujita, T. Takayanagi, and E. Tonni, *Aspects of AdS/BCFT*, *Journal of High Energy Physics* **11** (Nov., 2011) 43, [arXiv:1108.5152]. 42, 58, 59

[184] M. Nozaki, T. Takayanagi, and T. Ugajin, *Central charges for BCFTs and holography*, *Journal of High Energy Physics* **6** (June, 2012) 66, [arXiv:1205.1573]. 42, 58, 59

[185] G. Evenbly and G. Vidal, *Algorithms for Entanglement Renormalization: Boundaries, Impurities and Interfaces*, *Journal of Statistical Physics* (Apr., 2014) [arXiv:1312.0303]. 42, 49

[186] G. Evenbly and G. Vidal, *Quantum Criticality with the Multi-scale Entanglement Renormalization Ansatz*, *ArXiv e-prints* (Sept., 2011) [arXiv:1109.5334]. 44, 46

[187] O. Aharony, S. S. Gubser, J. Maldacena, H. Ooguri, and Y. Oz, *Large N field theories, string theory and gravity*, Phys. Rep. **323** (Jan., 2000) 183–386, [hep-th/9905111]. 44

[188] H. Nastase, *Introduction to AdS-CFT*, *ArXiv e-prints* (Dec., 2007) [arXiv:0712.0689]. 44

[189] A. V. Ramallo, *Introduction to the AdS/CFT correspondence*, *ArXiv e-prints* (Oct., 2013) [arXiv:1310.4319]. 44

[190] G. Evenbly and G. Vidal, *Tensor Network States and Geometry*, *Journal of Statistical Physics* **145** (Nov., 2011) 891–918, [arXiv:1106.1082]. 44

[191] N. Bao, C. Cao, S. M. Carroll, A. Chatwin-Davies, N. Hunter-Jones, J. Pollack, and G. N. Remmen, *Consistency conditions for an AdS multiscale entanglement renormalization ansatz correspondence*, Phys. Rev. D **91** (June, 2015) 125036, [arXiv:1504.06632]. 44

[192] R. Orus, *A Practical Introduction to Tensor Networks: Matrix Product States and Projected Entangled Pair States*, *Annals Phys.* **349** (2014) 117–158, [arXiv:1306.2164]. 46

[193] R. Orus, *Advances on Tensor Network Theory: Symmetries, Fermions, Entanglement, and Holography*, *Eur. Phys. J.* **B87** (2014) 280, [arXiv:1407.6552]. 46

[194] M. Hauru, G. Evenbly, W. W. Ho, D. Gaiotto, and G. Vidal, *Topological conformal defects with tensor networks*, Phys. Rev. B **94** (Sept., 2016) 115125, [arXiv:1512.03846]. 50, 51

[195] G. Evenbly and G. Vidal, *Tensor Network Renormalization*, *Physical Review Letters* **115** (Oct., 2015) 180405, [arXiv:1412.0732]. 51

[196] G. Evenbly and G. Vidal, *Tensor Network Renormalization Yields the Multiscale Entanglement Renormalization Ansatz*, *Physical Review Letters* **115** (Nov., 2015) 200401, [arXiv:1502.05385]. 51

[197] D. M. McAvity and H. Osborn, *Conformal field theories near a boundary in general dimensions*, *Nuclear Physics B* **455** (Feb., 1995) 522–576, [cond-mat/9505127]. 51, 54

[198] D. M. McAvity and H. Osborn, *Energy-momentum tensor in conformal field theories near a boundary*, *Nuclear Physics B* **406** (Oct., 1993) 655–680, [hep-th/9302068]. 51

[199] R. N. C. Pfeifer, G. Evenbly, and G. Vidal, *Entanglement renormalization, scale invariance, and quantum criticality*, Phys. Rev. A **79** (Apr., 2009) 040301, [arXiv:0810.0580]. 52, 57, 67

[200] G. Evenbly and G. Vidal, *Local Scale Transformations on the Lattice with Tensor Network Renormalization*, *Physical Review Letters* **116** (Jan., 2016) 040401, [arXiv:1510.00689]. 54

[201] C. Bachas, J. de Boer, R. Dijkgraaf, and H. Ooguri, *Permeable conformal walls and holography*, *Journal of High Energy Physics* **6** (June, 2002) 027, [hep-th/0111210]. 58

[202] H.-C. Chang and A. Karch, *Entanglement entropy for probe branes*, *Journal of High Energy Physics* **1** (Jan., 2014) 180, [arXiv:1307.5325]. 58

[203] K. Jensen and A. O'Bannon, *Holography, entanglement entropy, and conformal field theories with boundaries or defects*, Phys. Rev. D **88** (Nov., 2013) 106006, [arXiv:1309.4523]. 58

[204] J. Erdmenger, M. Flory, and M.-N. Newrzella, *Bending branes for DCFT in two dimensions*, *Journal of High Energy Physics* **1** (Jan., 2015) 58, [arXiv:1410.7811]. 58, 60

[205] C. Bachas, *Asymptotic symmetries of AdS2 Branes*, *ArXiv High Energy Physics - Theory e-prints* (May, 2002) [hep-th/0205115]. 58

[206] C. Bachas and M. Petropoulos, *Anti-de-Sitter D-branes*, *Journal of High Energy Physics* **2** (Feb., 2001) 025, [hep-th/0012234]. 58

[207] J. D. Brown and M. Henneaux, *Central charges in the canonical realization of asymptotic symmetries: An example from three dimensional gravity*, *Communications in Mathematical Physics* **104** (June, 1986) 207–226. 58

[208] B. Czech, L. Lamprou, S. McCandlish, B. Mosk, and J. Sully, *A stereoscopic look into the bulk*, *Journal of High Energy Physics* **7** (July, 2016) 129, [arXiv:1604.03110]. 62, 69

[209] J. de Boer, F. M. Haehl, M. P. Heller, and R. C. Myers, *Entanglement, holography and causal diamonds*, *Journal of High Energy Physics* **8** (Aug., 2016) 162, [arXiv:1606.03307]. 62, 69

[210] C. T. Asplund, N. Callebaut, and C. Zukowski, *Equivalence of emergent de Sitter spaces from conformal field theory*, *Journal of High Energy Physics* **9** (Sept., 2016) 154, [arXiv:1604.02687]. 62

[211] J.-d. Zhang and B. Chen, *Kinematic space and wormholes*, *Journal of High Energy Physics* **1** (Jan., 2017) #92, [arXiv:1610.07134]. 62

[212] C. Bény, *Causal structure of the entanglement renormalization ansatz*, *New Journal of Physics* **15** (Feb., 2013) 023020, [arXiv:1110.4872]. 62

[213] R. Sinai Kunkolienkar and K. Banerjee, *Towards a dS/MERA correspondence*, *ArXiv e-prints* (Nov., 2016) [arXiv:1611.08581]. 62

[214] D. Bak, M. Gutperle, and S. Hirano, *A dilatonic deformation of AdS_5 and its field theory dual*, *Journal of High Energy Physics* **5** (May, 2003) 072, [hep-th/0304129]. 63

[215] T. Azeyanagi, T. Takayanagi, A. Karch, and E. G. Thompson, *Holographic calculation of boundary entropy*, *Journal of High Energy Physics* **3** (Mar., 2008) 054, [arXiv:0712.1850]. 63

[216] M. Chiodaroli, M. Gutperle, and L.-Y. Hung, *Boundary entropy of supersymmetric Janus solutions*, *Journal of High Energy Physics* **9** (Sept., 2010) 82. 63

[217] D. Bak, M. Gutperle, and R. A. Janik, *Janus black holes*, *Journal of High Energy Physics* **10** (Oct., 2011) 56, [arXiv:1109.2736]. 63

[218] M. Gutperle and J. D. Miller, *Entanglement entropy at holographic interfaces*, Phys. Rev. D **93** (Jan., 2016) 026006, [arXiv:1511.08955]. 63

[219] D. Bak, C. Kim, K. K. Kim, H. Min, and J.-P. Song, *Geometric Monte Carlo and black Janus geometries*, *Physics Letters B* **767** (Apr., 2017) 341–346, [arXiv:1611.10255]. 63

[220] V. Balasubramanian, P. Kraus, and A. Lawrence, *Bulk versus boundary dynamics in anti-de Sitter spacetime*, Phys. Rev. D **59** (Feb., 1999) 046003, [hep-th/9805171]. 65

[221] F. Pastawski, B. Yoshida, D. Harlow, and J. Preskill, *Holographic quantum error-correcting codes: toy models for the bulk/boundary correspondence*, *Journal of High Energy Physics* **6** (June, 2015) 149, [arXiv:1503.06237]. 68

[222] Z. Yang, P. Hayden, and X.-L. Qi, *Bidirectional holographic codes and sub-AdS locality*, *Journal of High Energy Physics* **1** (Jan., 2016) 175, [arXiv:1510.03784]. 68

[223] P. Hayden, S. Nezami, X.-L. Qi, N. Thomas, M. Walter, and Z. Yang, *Holographic duality from random tensor networks*, *Journal of High Energy Physics* **11** (Nov., 2016) 9, [arXiv:1601.01694]. 68

[224] A. Bhattacharyya, Z.-S. Gao, L.-Y. Hung, and S.-N. Liu, *Exploring the tensor networks/AdS correspondence*, *Journal of High Energy Physics* **8** (Aug., 2016) 86, [arXiv:1606.00621]. 68

[225] W. Donnelly, D. Marolf, B. Michel, and J. Wien, *Living on the edge: a toy model for holographic reconstruction of algebras with centers*, *Journal of High Energy Physics* **4** (Apr., 2017) #93, [arXiv:1611.05841]. 68

[226] J. Erdmenger, M. Flory, C. Hoyos, M.-N. Newrzella, and J. M. S. Wu, *Entanglement entropy in a holographic Kondo model*, *Fortschritte der Physik* **64** (Jan., 2016) 109–130, [arXiv:1511.03666]. 68

[227] A. Karch, J. Sully, C. F. Uhlemann, and D. G. E. Walker, *Boundary Kinematic Space*, *ArXiv e-prints* (Mar., 2017) [arXiv:1703.02990]. 69

[228] P. Hayden, R. Jozsa, D. Petz, and A. Winter, *Structure of States Which Satisfy Strong Subadditivity of Quantum Entropy with Equality*, *Communications in Mathematical Physics* **246** (2004) 359–374, [quant-ph/0304007]. 75

[229] W. Israel, "Singular hypersurfaces and thin shells in general relativity," Nuovo Cim. B **44S10**, 1 (1966) [Nuovo Cim. B **44**, 1 (1966)] Erratum: [Nuovo Cim. B **48**, 463 (1967)]. 59, 72

[230] G. Evenbly, talk given at Perimeter Institute, October 2011 https://www.perimeterinstitute.ca/images/conferences/tensor_glen_evenbly.pdf. 53